DOI:10.14753/SE.2015.1802

STUDIES ON MODULATED ELECTROHYPERTHERMIA INDUCED TUMOR CELL DEATH IN A COLORECTAL CARCINOMA MODEL

PhD thesis

Nóra Meggyesházi M.D.

Pathological Sciences Doctoral School

Semmelweis University

Supervisor: Dr. Tibor Krenács Ph.D.

Official reviewers:
Dr. Tibor Glasz Ph.D.
Dr. Gyula Péter Szigeti Ph.D.

Head of the Final Examination Committee:
Dr. Péter Sótonyi Member of MTA.

Members of the Final Examination Committee:
Dr. Gábor Lotz Ph.D.
Dr. Árpád Csurgay Member of MTA

Budapest, 2015

DOI:10.14753/SE.2015.1802

1. TABLE OF CONTENT

DOI:10.14753/SE.2015.1802

DOI:10.14753/SE.2015.1802

DOI:10.14753/SE.2015.1802

2. ABBREVIATIONS

AEC	aminoethylcarbazole
AIF	apoptosis inducing factor
Apaf 1	apoptotic protease activating factor 1
APC	antigen presenting cell
AsPC-1	human pancreatic cell line
ATP	adenosine triphosphate
Bag3	Bcl-2-associated athanogene 3
Bak	Bcl-2 homologous antagonist/killer
Bax	Bcl-2 associated X protein
Bcl-2	B-cell lymphoma 2
BID	BH3 interacting-domain death agonist
BSA	bovine serum albumin
CD	cluster of differentiation
CHPP	continous hyperthermic peritoneal perfusion
CRT	calreticulin
DC	dendritic cell
DAB	3,3’ diaminobenzidine
DAMP	damage associated molecular pattern
DAPI	4’,6 diamidino-2-phenylindole
dATP	deoxyadenosine triphosphate
DMEM	Dulbecco’s modified Eagle’s minimal essential medium
DNA	deoxyribonucleic acid
DNAJB	DnaJ (Heat shock protein 40) homolog, subfamily B
DIABLO	direct IAP-binding protein with low pI
dUTP	2'-deoxyuridine 5'-triphosphate
ECL	electrochemiluminescence
EDTA	ethylenediaminetetraacetic acid
ER	endoplasmic reticulum
FADD	Fas-associated protein with death domain
FASL	Fas ligand

FCS	fetal calf serum
FFPE	formalin-fixed paraffin-embedded
FOV	field of views
HIPEC	hyperthermic intraperitoneal chemotherapy
HMGB1	high mobility group box 1
HRP	horseradish peroxidase
HSF	heat shock factor
Hsp70	heat shock protein 70
Hsp90	heat shock protein 90
HSPA	heat shock protein 70 A
HT29	human colorectal adenocarcinoma cell line
HTRA2	high temperature requirement protein A2
H&E	hematoxylin and eosin
IAP	inhibitor of apoptosis
ICD	immunogenic cell death
Ig	immunogloubulin
log2FC	binary logarithm of fold change
mEHT	modulated electrohyperthermia
MHC	major histocompatibility complex
MIAME	Minimum information about a microarray experiment
MIAPaCa-2	human pancreatic cell line
min/h	minute per hour
MLS	mitochondrial localization signal
MMP	mitochondrial membrane permebilization
MPO	myeloperoxidase
mRNA	messenger ribonucleic acid
NF-κB	nuclear factor kappa-light-chain-enhancer of activated B cells
NK	natural killer
PS	phosphatidilserin
PVDF	polyvinylidene difluoride
RAGE	receptor advanced glycation endproducts
RIN	RNA integrity number

RIP1	receptor-interacting serine/threonine-protein kinase 1
RIP3	receptor-interacting serine/threonine-protein kinase 3
rMA	relative mask area
RNA	ribonucleic acid
ROS	reactive oxygen species
SAM	significance analysis of microarrays
SAR	specific absorption rate
SAS	human tongue squamous cell carcinoma cell line
SDS-PAGE	sodium dodecylsulfate polyacrylamide gel
tBID	truncate BH3 interacting-domain death agonist
TBS	Tris-buffered saline
TDE	tumor destruction efficiency
TDR	tumor destruction ratio
TdT	terminal deoxynucleotidyl transferase
TER	thermal enhancement ratio
TIM3	T-cell immunoglobulin domain and mucin domain 3
TLR2/4	Toll like receptor 2/4
TMA	tissue microarray
TNFα	tumor necrosis factor α
TNFα-R1	tumor necrosis factor α receptor 1
TRAIL	TNF-related apoptosis-inducing ligand
TRAIL-R1	TNF-related apoptosis-inducing ligand receptor 1
TRAIL-R2	TNF-related apoptosis-inducing ligand receptor 2
TUNEL	terminal deoxynucleotidyl transferase dUTP nick end labeling
WBH	whole body hyperthermia
WGA	wheat germ agglutinin
ε_k	complex permittivity
σ_k	complex conductivity
ΔT	temperature difference
Δt	time difference
E_{loc}	average local electric field
ρ	density of a material

DOI:10.14753/SE.2015.1802

3. INTRODUCTION

3.1. Characteristics of hyperthermia in oncology

The term hyperthermia in oncology refers to techniques of heat application administered to tissues as an adjunct to conventional strategies of cancer treatment such as chemo- or radiotherapy. (Hildebrandt et al. 2002). The aim of hyperthermia treatment is, like any oncological therapies, to completely and selectively destroy the malignant tissue (Szasz et al. 2010). Hyperthermia is mostly identified with a range of temperature of the target between 40-48°C maintained at a treated site for a period of one hour or more each time (Chicheł et al. 2007). From this loose definition it becomes clear that this is a rather heterogeneous group of treatments with diverse efficiency and outcome depending on the source of heat generation and the histogenesis, differentiation, site/microenvironment and the defective regulatory pathways of the treated tumors.

3.1.1. Forms of hyperthermia

The main forms of hyperthermia include whole body hyperthermia, hyperthermic perfusion techniques and local/regional hyperthermia (Hildebrandt et al. 2002).

Whole body hyperthermia (WBH) is used for patients with metastatic disease usually in combination with chemotherapy. It can be performed by thermal chambers, hot water blankets or infrared radiators. In extreme WBH the patient core temperature is heated up to 42°C for 60 minutes under general anesthesia or deep sedation, while in moderate WBH the patient core temperature is heated up between 39.5-41°C for 3-4 hours (Chicheł et al. 2007). A few phase II studies were carried out using WBH in combination with chemotherapy. WBH was applied with oxaliplatin, leucovorin and 5-fluorouracil treating patients with metastatic rectal tumors with a 20% response rate (Hegewisch-Becker et al. 2002). Recurrent ovarian cancer and recurrent and metastatic ovarian cancer patients were treated with WBH in combination with carboplatin with a response rate of 45% (Atmaca et al. 2009) and 33% (Richel et al. 2004) respectively. The phase II study of metastatic soft tissue sarcoma patients treated with WBH in combination with fosfamide, carboplatin and etoposide revealed a 28.4% response rate (Westermann et al. 2003).

Hyperthermic perfusion techniques include hyperthermic isolated limb perfusion and hyperthermic intraperitoneal perfusion with or without administering a chemotherapy agent (hyperthermic intraperitoneal chemotherapy- HIPEC, continuous hyperthermic peritoneal perfusion- CHPP) (Wust et al. 2002; Chicheł et al. 2007). HIPEC proved to be beneficial for patients with peritoneal cacinomatosis from appendicial cancer, colorectal cancer, ovarium cancer and peritoneal mesothelioma (Chua et al. 2009). The median survival was found to be between 26 to 56 months in ovarian cancer with peritoneal carcinomatosis when cytoreductive surgery was used with HIPEC (Chua et al. 2009). In colorectal cancer with peritoneal carcinomatosis the median disease specific survival was found to be 22.2 months when cytoreductive surgery was applied with HIPEC while it was 12.6 months in the control arm (Aoyagi et al. 2014). Hyperthermic isolated limb perfusion is a technique bypassing a large supplying artery and a vein of a limb to deliver heat to drained blood in an extra corporal way (Chicheł et al. 2007). This method has fewer side effects than WBH, mostly administered in combination of chemotherapy in melanomas or soft tissue sarcomas (Chicheł et al. 2007). Hyperthermic isolated limb perfusion may be used to treat malignant melanomas with an overall median response rate of 90% (Moreno-Ramirez et al. 2010) or soft tissue sarcomas with an overall response rate of 81.5% (Trabulsi et al. 2012).

Local hyperthermia is applied to tumors of relatively small size, while regional hyperthermia is used to heat up a body region involving the tumor. For such heating infrared radiation, microwaves, radio waves and ultrasound can be used (Szasz et al. 2002; Chicheł et al. 2007). The following sections will briefly summarize what is known about the biophysical background, major characteristics and utilization for cancer treatment of local hyperthermia.

3.1.2. Theoretical background of local hyperthermia

Oncological hyperthermia uses heat energy to destroy the malignant cells. The absorbed energy is converted to heat, which further leads to increment on temperature. Therefore, one has to distinguish heat (as the absorbed energy) and the resulted elevation of temperature as a consequence of energy absorption. Local/regional hyperthermia works by energy/heat absorption in the targeted tissue volume. Although, blood flow can reduce the

efficiency of energy absorption by cooling the heated volume incorporating the tumor tissue (Szasz et al. 2010).

3.1.3. Pre-clinical observations and results

To provoke the cytotoxic effect of hyperthermia either *in vitro or in vivo,* usually a water bath is applied for generating heat within a therapeutic range of temperature and duration. For example human head and neck squamous cell carcinoma cell line xenografted to the hind leg of BALB/cA Jcl-nu mice, (Tamamoto et al. 2003) or HT29 human colorectal carcinoma cell line xenografted to NCI Nu/nu mice (Sun et al. 2008) or HT29 xenografted to BALB/C nu/nu mice were tested in this way (Liang et al. 2007).

Hyperthermia can inhibit DNA, RNA and protein synthesis during the treatment, but RNA and protein synthesis rapidly recover after the treatment (Hildebrandt et al. 2002). The DNA synthesis is inhibited due to denaturation of proteins involved in DNA repair such as DNA-polymerase α and β and Rad51 (Hildebrandt et al. 2002; Genet et al. 2013). Heat can change the fluidity of the cell membrane resulting in the softening or melting of the lipid bilayer. This leads to the accumulation of cholesterol and ceramide in the lipid layer resulting in the rearrangement of the lipid rafts with concomitant changes in the protein content such as phospholipase A2 and phospholipase C causing either calcium release from the ER or the transcriptional activation of heat shock proteins (Hsp) (Csoboz et al. 2013). The heat stress related to hyperthermia on the other hand may induce heat shock protein (Hsp) synthesis through protein aggregation and denaturation followed by heat shock factor (HSF) binding to the promoter regions of different Hsp's (Hildebrandt et al. 2002). The elevated intracellular Hsp concentration can be cytoprotective (Horvath et al. 2010), may translocate to the cytoplasm membrane, where it either protects the cell (Horvath et al. 2010) or act as an immunostimulant (Nishida et al. 1997; Hildebrandt et al. 2002).

Hyperthermia can lead to necrosis and programmed cell death in a tremperature dependent manner in a murine mastocytoma cell line (Harmon et al. 1990) and in several hematological tumor cell lines (Harmon et al. 1990; Baxter et al. 1992; Gabai et al. 1995; Yonezawa et al. 1996). However, hyperthermia *in vivo* is usually used for targeting solid tumors. Unfortunately the anti-tumor efficiency of hyperthermia can vary depending on the

models used. Hyperthermia for 1h at 43.5°C induced DNA fragmentation 6h post-treatment in Dunn osteosarcoma cell line (Rong et al. 2000) and for 44 min on 44°C in human tongue squamous cell carcinoma cell line (SAS) (Kajihara et al. 2008). On the other hand hyperthermia was not found to be effective either at 42°C in colorectal cancer cell line (HT29) (Shchepotin et al. 1997), or at 43°C when used for 1h in pancreatic cancer cell lines (AsPC-1, MIAPaCa-2) (Adachi et al. 2009). *In vivo* however, instead of water bath infrared radiation, microwave or radiofrequency is applied for generating heat.

Beside the cellular and cytotoxic effects, hyperthermia can regulate blood flow by elevating blood flow/perfusion up to ~42^{o}C and reducing it above 42°C. This can be exploited in combination with chemotherapy for elevating the local concentration of chemotherapeutic agents by moderate hyperthermia (Hildebrandt et al. 2002).

3.1.4. Clinical observations

Hyperthermia is usually applied in combination with radiotherapy, chemotherapy or both. As mentioned above hyperthermia below 42°C can increase the blood flow, which is reduced above this temperature. In clinical conditions local/regional hyperthermia in most of the cases does not exceed 42°C, therefore, this is the basis of combinational therapy (Hildebrandt et al. 2002). When hyperthermia and radiation therapy act synergistically the term "thermal radiosenzitization" is used, which is most prominent in S-phase proliferating cell fractions that are usually resistant to radiotherapy (Hildebrandt et al. 2002). To define the benefit of the combinational therapy thermal enhancement ratio (TER, the quotient of survival fraction of cells treated with radiation alone or with radiation and hyperthermia in combination) is used (Overgaard 1984; Hildebrandt et al. 2002). Hypoxic cells, cells with impaired nutrient supply and/or acidic pH, react sensitively to combined therapy of heat and radiation (Dewey et al. 1977; Dewey 1994). Synchronous application of the combined therapy would be the best routine; however, technical difficulties still need to be overcome for this to be carried out. Therefore, in clinical practice heat and radiation are applied after one and other within a short period of time. Some prefer applying radiation first followed by heat within 2-4 hours, while others apply heat prior to irradiation. So far, neither of these strategies has been tested by randomized clinical studies (Hildebrandt et al. 2002).

The term “thermal chemosenzitization” is used in analogy with thermal radiosensitization, for indicating synergy between hyperthermia and chemo- or radiotherapy. The applicability of chemotherapeutic agents in combination with hyperthermia depends on pharmacokinetic properties of the drug. For example drugs which are metabolized in the liver should be applied a few hours before hyperthermia (e.g.: cyclophosphamide, ifosfamide). One would expect that changes in tumor blood supply will affect the distribution of the drug in the malignant tissue. In reality, this interaction is highly complex and depends much more on environmental factors such as fluid balance and pH in addition to blood supply, than radiation and heat (Hildebrandt et al. 2002).

So far a few randomized trials have been carried out i.e. where hyperthermia was combined with radiotherapy of head and neck tumors and breast cancers with a complete response rate of 32% with hyperthermia and 30% without hyperthermia, (Perez et al. 1991; Hildebrandt et al. 2002). Hyperthermia was used together with chemotherapy of soft tissue sarcomas with a response rate of 28.8% in the combination group and 12.7% in the chemotherapy group (Issels et al. 2010). A phase II study was performed on locally advanced rectal tumors (T4) with an 83% disease free survival in the 24.9 months median follow up time. (Barsukov et al. 2013).

3.2. Principles of modulated electrohyperthermia

Modulated electrohyperthermia (mEHT), a subtype of local/regional hyperthermia, is a non-invasive technique for targeted tumor treatment using 13.56 MHz radiofrequency with 1/f amplitude modulation. Besides the thermal effect of the electric field generated by mEHT, the electric field itself also has a tumor destructing effect (Andocs et al. 2009), however its mechanism of action has not been described yet.

DOI:10.14753/SE.2015.1802

3.2.1. Bioelectrodynamic description of tissues

3.2.1.1. Conditions and variables

Biological materials can be described by complex permittivity and complex conductivity (Mátay et al. 2000).

Complex permittivity (ε_k) is related to the dipole content of the biological material, due to the cytoplasmic and extracellular macromolecules and the membrane bound macromolecules. Tissue molecules as dipoles will rotate upon the influence of an exciting electric field. This rotation will be asynchronous with the electric field due to the inertia and the internal friction of the dipoles, this is called dielectric relaxation, which is time dependent. This relaxation results in dispersion which is highly frequency dependent (Mátay et al. 2000). The relaxation can be described by more than one relaxation constants α, β, γ and δ (**Figure 1)**. Each domain is determined by relaxation frequencies. α dispersion (< 1 kHz) can be explained by the cell membrane capacitance. The capacitance decreases from 20 μF/cm^2 to 1 μF/cm^2 with the elevation of the frequency (1 Hz - 1 kHz.) This decrement is caused by the elevated ion current through the plasma membrane. β dispersion (1 kHz-10 MHz) is related to the accumulation of the dielectric material on the cell membrane surface. γ dispersion (in the GHz range) is linked with the relaxation of the bound water (Blad et al. 1996; Mátay et al. 2000; Zou et al. 2003). A small δ dispersion exists between β and γ dispersion frequencies (not visible in **Figure 1**), related to bound water on the macromolecules and the charged proteins (Schwan 1957; Mátay et al. 2000).

Besides dipoles, biological materials also contain free charges which can drift upon influence by the electric field. To describe this drifting we use the term complex conductivity (σ_k), which is also frequency dependent (**Figure 1**) (Mátay et al. 2000).

The interference between radiofrequency field and the biological material can result in thermal and non-thermal effects. The thermal effect is related to the rotation of dipoles and the concomitant friction, resulted in electric displacement of the electric field (Mátay et al. 2000).

The permittivity and the conductivity are characteristic to the biological material itself and not the electric circuit (Mátay et al. 2000).

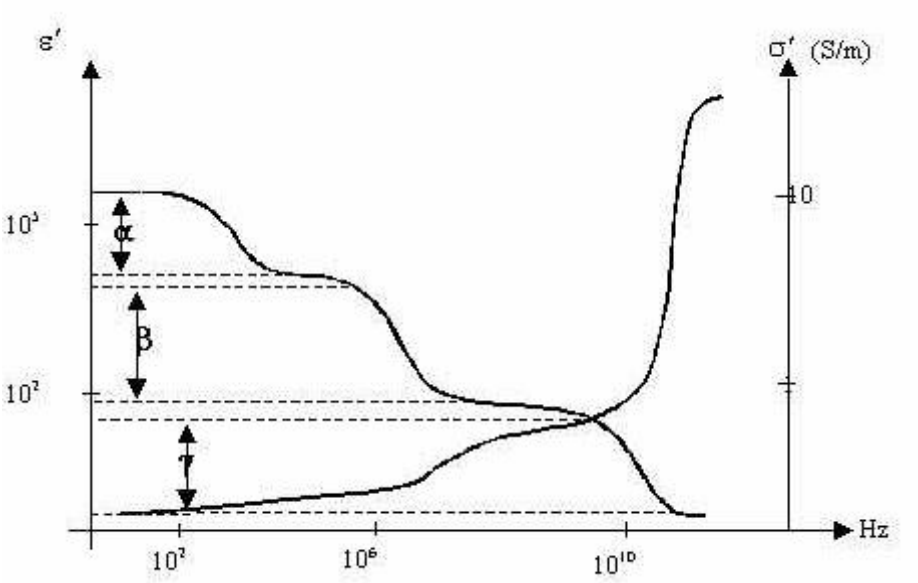

Figure 1. The frequency dependent relaxation of real part of permittivity and the frequency dependency of the real part of conductivity. The graph is showing the real part of complex permittivity relaxation, pointing out α, β and γ dispersion and real part of complex conductivity. ε' is the real part of complex permittivity, σ' is the real part of complex conductivity [S/m], while the 'x' axis is the frequency of the applied field. (Scholoz et al. 2000)

As a summary in all biological materials bioelectrodynamic properties can be simplified to the description of complex permittivity (ε_k) (resulted from the dipole content), complex conductivity (σ_k) (resulted from the free charges) and to the dispersion properties (resulted from the distinct relaxation at different frequencies) (Mátay et al. 2000; Szasz et al. 2010).

3.2.1.2. Bioelectrodynamic characteristics of malignancies

As it was mentioned above the dielectric permittivity and the complex conductivity of tissues are highly frequency dependent. As it is characteristic to the material itself, different biological materials (tissues) have clearly different bioelectric properties (σ and ε). In the liver conductivity is 0.15 S/m at 10kHz, 0.16 S/m at 100kHz, 0.47 S/m at 10MHz and 0.9 S/m at 100MHz. In the lung it is 0.11 S/m at 10kHz, and 0.8 S/m at 100MHz. In the spleen it is 0.62 S/m at 100kHz, 0.84 S/m at 10MH and 1.05 S/m at 100MHz. In the kidney it is 0.24 S/m at 100kHz, 0.64 S/m at 10MHz and 0.94 S/m at 100MHz. It is obvious for

example that the conductivity of the spleen is higher than that of the liver or the lung. The difference of σ or ε between the different tissues on diverse frequencies is not linear. (Foster 2000; Raoof et al. 2013)

If we compare the bioelectric properties of malignant and non-malignant tissues at the same frequency, malignant tumors show higher permittivity (ε) and conductivity (σ) than normal tissues (Pethig et al. 1984; Blad et al. 1996; Zou et al. 2003; O'Rourke et al. 2007). For example, in breast tissue in the range of 3MHz-3GHz, σ of the normal tissue increases from 1.5 to 3 mS/cm, while σ of malignant breast tumors increases from 7.5-12 mS/cm, while ε of the normal tissue remains 10 and of the malignant it increases from 50 to 400. There is a 4-fold increase in conductivity and 5 to 40 fold increase in permittivity for the benefit of tumors compared to normal tissues (Zou et al. 2003).

The elevated conductivity can be explained by the altered metabolism of the tumor cells. This is called aerobic glucolysis or the Warburg effect. The high rate of glucose uptake and lactate production results in an increased ion concentration and concomitant increased conductivity (Szasz et al. 2010). On the other hand the altered electrical properties of malignant tissue are attributed to increased cellular water and salt content, as well as altered membrane permeability of the tumor cells (Pethig et al. 1984; Blad et al. 1996; Scholoz et al. 2000; Zou et al. 2003; O'Rourke et al. 2007).

3.2.2. Biophysical background of modulated electrohyperthermia

Modulated electrohyperthermia is a non-invasive technique using capacitive coupled (the targeted tissue is put between the condenser electrodes) 13.56 MHz radiofrequency with 1/f amplitude modulation to target tumor tissue.

This specific frequency is used because of the following reasons. The applied radiofrequency has to penetrate deeply into and across the body. The penetration depth depends on the frequency used, as well as permittivity and conductivity of the targeted tissue. Therefore, at a fixed frequency the penetration depth is higher e.g. through the same thickness of homogenous fat than of homogenous muscle (Cheung 1982). In order to ensure that capacitive coupled radiofrequency penetrates into and across the average human body thickness the frequency has to be below 25 MHz (Szasz et al. 2010). The applied

frequency has to be safe, not to trigger nerve excitation, preferable to be between 10 kHz and 1 GHz (Szasz et al. 2010) and has to be in the range of β dispersion (around 10 MHz) to influence cell membranes including their embedded receptors (Szasz et al. 2010). It is also practical to be in a free frequency range, which does not need shielding for avoiding interference with other electronic devices. All these criteria meet at 13.56 MHz (Szasz et al. 2010).

The selectivity of mEHT is based on the difference in σ and ε values between malignant and non-malignant tissue on 13.56 MHz. Significant difference in these values was found among breast cancer, pancreatic carcinoma, and hepatocellular carcinoma cell lines but in all cases both the permittivity and conductivity significantly exceeded of those found in the related normal cells (Zou et al. 2003; Raoof et al. 2013).

The thermal effect of the electromagnetic field is associated with the absorbed energy by the tissue; it is described by the specific absorption rate (SAR) (Mátay et al. 2000).

$$SAR = \frac{\sigma}{\rho} E_{loc}^2 \qquad (1)$$

where σ is the conductivity, ρ the density of the material, while E_{loc} is the average local electric field.

Changes in the temperature, as a thermal effect, can be described by the following:

$$\Delta T = \frac{1}{C} SAR \Delta t \qquad (2)$$

where ΔT is the temperature difference in Δt time difference and C is the specific heat of the biological material.

Therefore SAR can be used as the dose of the thermal effect of electromagnetic field.

On the other hand, in the interaction between the electric field and the biological material a non-thermal (or non temperature dependent) effect can also be described related to the non thermal equilibrium (Mátay et al. 2000). It was shown that mEHT has such effect on HT29 (human colorectal adenocarcinoma cell line) cancer xenograft model, where the thermal

and non-thermal effects act in synergy for tumor destruction, but the molecular mechanism of these effects were not explained (Andocs et al. 2009).

3.2.3. Clinical observations using modulated electrohyperthermia

So far, mainly the thermal effect is taken into consideration when mEHT is used in clinical practice. Therefore, mEHT represents a heating method in hyperthermic oncology.

There have been several case reports and retrospective studies published on the benefits of using hyperthermia for anti-tumor therapy (Szasz et al. 2010). Though mEHT treatment can interfere with tumor tissue in monotherapy it has been used for hyperthermic oncology in phase I and phase II clinical studies in combination with chemo- and/or radiotherapy of brain, liver, breast and gastrointestinal malignancies (Brazma et al. 2001; Fiorentini et al. 2006; Fiorentini et al. 2006; Wismeth et al. 2010). For instance, compared to the published 30-33 weeks median overall survival, temozolomide-based chemotherapy and radiotherapy supported with mEHT resulted in 36 weeks median overall survival (n = 12) with one complete and two partial remissions (response rate 25%) in recurrent malignant gliomas (Fiorentini et al. 2006). Also, fluorouracil based chemotherapy combined with mEHT resulted in 24.1 months median overall survival in liver metastatic primary colorectal cancers (n = 90) compared to the 12 month median survival reported when fluorouracil chemotherapy was used alone (Hager et al. 1999). Also, it has already been used in combination with chemo– and radiotherapy with benefit for treating recurrent breast cancer (Feyerabend et al. 2001).

3.3. Theoretical background of the observed biological impact of hyperthermia

Several studies have proven that hyperthermia can cause different cell death forms under various programmed cell death subroutines (e.g. caspase dependent apoptosis or autophagic cell death) and accidental necrosis at a heat absorption dependent manner (Hildebrandt et al. 2002). *In vitro* circumstances caspase dependent programmed cell death was proven in cervical cancer cell line and in osteosarcoma cell line (Zhou et al. 2011; Hou et al. 2014). Hyperthermia induced DNA fragmentation was found in human head and neck squamous cell carcinoma cell line and in murine fibrosarcoma cell line *in vitro* without further

specifying the exact programmed cell death subroutine (Tamamoto et al. 2003; Lui et al. 2010). In HT29 cell line *in vitro* cell death subroutines were contradictory (Chen et al. 2008; Makizumi et al. 2008) though *in vivo* the upregulation of Bax protein was found without further clarifying the cell death mechanism (Liang et al. 2007). Accordingly, hyperthermia related cell death mechanism needs to be specified *in vivo* in different tumor types.

3.3.1. Characteristics of cell death forms

For the definition of different type of cell death forms we first have to define the first irreversible phase within cell damage, the so called "point of no return" and then the characteristics of a dead cell.

The "point of no return" in a cell's fate can usually be characterized by (1) a massive caspase activation, which is part of the classic apoptotic program. However, caspase independent death may also occur, moreover, caspases might also be involved in non-lethal pathways such as cell differentiation and activation. Further feature is the loss of mitochondrial transmembrane potential (2), which is usually preceded by mitochondrial membrane permeabilisation (MMP). The complete MMP (3) results in the liberation of lethal catabolic enzymes or activators. Finally, the phosphatidilserin (PS) exposure (4) from the inner to the outer leaflet of the plasma membrane can also be a sign of irreversible cell damage (Kroemer et al. 2005; Kroemer et al. 2009).

The main characteristics of cell death are: loss of plasma membrane integrity (1); blebbing of the cytoplasmic membranes and shrinkage of nuclear chromatin followed by the complete fragmentation of the cell including the nucleus (2); the occurrence of discrete nuclear bodies (referred to as "apoptotic bodies") (3) and finally, the engulfment of cells' corps by adjacent cells or phagocytes (4) *in vivo* (Kroemer et al. 2005; Kroemer et al. 2009).

Several subroutines of programmed cell death forms exist including apoptosis, necroptosis/regulated necrosis, autophagic cell death, mitotic catastrophe, netosis, parthantos, pyroptosis, anoikis, entosis and cornification (Galluzzi et al. 2012).

Apoptosis was first described as a specific morphological aspect of cell death by Kerr in 1972 (Kerr et al. 1972; Elmore 2007). It was first investigated occurring during the development of Caenorhabiditis elegans, which is made up of 1090 somatic cells in an adult worm of which 131 undergoes the apoptotic process during development (Elmore 2007). The morphological signs of apoptosis are reduction of cellular volume (pycnosis), chromatin condensation, nuclear fragmentation (karyorrhexis), plasma membrane blebbing (Elmore 2007; Kroemer et al. 2009; Galluzzi et al. 2012). For the molecular characterization we have to differentiate extrinsic and intrinsic apoptosis, which can be caspase dependent and independent (Galluzzi et al. 2012). Extrinsic apoptosis can be initiated by a death ligand (e.g. FASL, TNFα and TRAIL) through death receptors (e.g. FAS, TNFα-R1, TRAIL-R1 and TRAIL-R2). Alternatively, extrinsic apoptosis can also be initiated by dependence receptors (netrin receptors) which exert lethal functions when the concentration of their specific ligand falls below a critical threshold (Galluzzi et al. 2012).

Extrinsic apoptosis would undergo one of the three major signaling cascades: (1) death receptor signaling, activation of caspase-8 followed by the activation of the effector caspase-3 or (2) death receptor signaling activation of caspase-8 cleavage of BID (tBID) resulting in MMP followed by caspase-9 and caspase-3 activation. Ligand deprivation-induced dependence receptor signaling (3) followed by caspase-9 and caspase-3 cascade activation (Galluzzi et al. 2012).

Intrinsic apoptosis can be triggered by intracellular stress such as DNA damage, oxidative stress, cytosolic Calcium overload, accumulation of unfolded proteins in the endoplasmic reticulum (ER), radiation, hypoxia, hyperthermia, viral infection or free radicals (Elmore 2007; Galluzzi et al. 2012). As a result of intracellular stress pores are formed in the mitochondria membrane leading to release of intermembrane space proteins to the cytoplasm (Elmore 2007; Galluzzi et al. 2012). The mechanism of pore formation can be achieved by induction of mitochondrial permeability transition, in which non-specific pores are opened in the outer and the inner membranes of the mitochondria. This can occur in both programmed cell death and accidental necrosis (Gogvadze et al. 2006). The second option for pore formation is the outer membrane permeabilisation by Bcl2 (B-cell lymphoma 2) family pro-apoptotic proteins, such as Bax (Bcl-2 associated X protein) and

Bak (Bcl-2 homologous antagonist/killer) occurring in the apoptotic cascades (Gogvadze et al. 2006; Galluzzi et al. 2012). Also, hypotonicity and the modulation of ionic fluxes can lead to mitochondrial membrane permeabilisation (Gogvadze et al. 2006). Once the pores are formed, the mitochondrial transmembrane potential decreases and the intermembrane space proteins are released to the cytosol, such as cytochrome c, apoptosis inducing factor (AIF), endonuclease G, direct IAP-binding protein with low pI (DIABLO) and high temperature requirement protein A2 (HTRA2) (Galluzzi et al. 2012).

If the intermembrane space protein release is followed by a caspase dependent subroutine, then the cytochrome c and Apaf1 (Apoptotic protease activating factor 1) (with d9ATP) will form the apoptosome, which will further trigger the activation of pro-caspase-9 and the effector cascase-3.

On the other hand mitochondrial AIF and endonuclease G can also tranaslocate to the cell nucleus, where they can mediate large scale DNA fragmentation on a caspase independent manner. AIF is synthesized in the cytoplasm as a 67 kDa protein with a mitochondrial localization signal (MLS) in the N terminus. Once it is imported to the mitochondria MLS is removed resulting in a 62 kDa mature protein. During the mitochondrial pore formation a soluble 57 kDa fragment is cleaved form AIF, released from the intermembrane space and transferred to the nucleus (Norberg et al. 2010). Although AIF does not have a canonical DNA binding domain but has a positive charged surface which can bind to the negative charged phosphate backbone of the DNA (Natarajan et al. 2012).

For a long time, necrosis was only considered as an accidental cell death mechanism, however, it can occur also in a regulated manner referred to as programmed necrosis (Galluzzi et al. 2012). It can be triggered by the same ligands and receptors as extrinsic apoptosis (Denecker et al. 2001; Nicotera 2002; Christofferson et al. 2010; Vandenabeele et al. 2010; Han et al. 2011), but caspases are inhibited, therefore RIP1 (receptor interacting serin/threonin-protein kinase 1) and RIP3 (receptor interacting serin/threonin-protein kinase 1) are not degraded and activate the execution of regulated necrosis (Galluzzi et al. 2012). RIP1 can be activated by autophosphorilation on Ser161 and dimerization. RIP3 can be phosphorilated on Ser199 leading to its activation (Christofferson et al. 2010). Regulated necrosis can occur on RIP1 dependent manner or RIP3 dependent but RIP1 independent

manner (Galluzzi et al. 2012). Although the initiation of necroptosis is known the downstream execution mechanism is still unclear (Christofferson et al. 2010; Vanlangenakker et al. 2012).

Autophagic cell death is characterized by a massive cytoplasmic vacuolization. This kind of cell death can be related to some types of cancers which lack modulators like Bax, Bak or caspases. In most cases autophagy acts as a cytoprotective response, only when it fails to protect the cell it turns into a cell death mechanism (Galluzzi et al. 2012).

3.3.2. Characteristics of immunogenic cell death forms

Apoptosis was considered as an immunologically silent form of cell death, however, recently it has been revealed that some lethal stimuli can lead to an immunogenic way of cell death (Kroemer et al. 2009; Krysko et al. 2012). Immunogenic cell death (ICD) is a form of programmed tumor cell death. In overlap with the molecular signs of programmed cell death the spatiotemporal occurrence of the damage associated molecular pattern (DMAP) is required for professional antigen presenting cells to trigger an antitumor immune response. (Scheffer et al. 2003; Ullrich et al. 2008; Kepp et al. 2011; Garg et al. 2012; D'Eliseo et al. 2013; Ladoire et al. 2013). ICD is known to be provoked by massive cell stress in synergy with programmed cell death (Kepp et al. 2009; D'Eliseo et al. 2013; Krysko et al. 2013; Ladoire et al. 2013) triggered by chemotherapeutic agents (doxorubicin, oxaliplatin etc.) (Tesniere et al. 2010; Ladoire et al. 2013), cardiac glycosides (Menger et al. 2012), hypericin based photodynamic therapy (Castano et al. 2006; Mroz et al. 2011; Garg et al. 2012) or capsaicin (D'Eliseo et al. 2013). It is of note, however, that these interventions can generate slightly different DAMP patterns (Garg et al. 2013; Kroemer et al. 2013).

The DAMP sequence, relevant to induce ICD in tumor cells include the pre-apoptotic surface exposure of calreticulin (CRT), the surface appearance of heat shock proteins (Hsp70 and Hsp90) and ATP release at early apoptotic stages, followed by passive release of high mobility group box 1 (HMGB1) as well as Hsp70 and Hsp90 at the late stages (Garg et al. 2010; Kepp et al. 2011; Garg et al. 2012; Martins et al. 2012; D'Eliseo et al. 2013; Garg et al. 2013; Ladoire et al. 2013).

Calreticulin is mainly located in the endoplasmic reticulum, interacting with ERp57 and calnexin to maintain the proper protein folding. In the cytoplasm membrane ecto-calreticulin, located in the lipid rafts, act as an ‘eat me‘ signal, where its life time is around 12h. The calreticulin exposure occurs before any sign of an apoptotic event, however an apoptotic signal is required for this exposure. It is suggested that mitochondrial dysfunction and reactive oxygen species (ROS) production with secondary endoplasmic reticulum stress or local ROS generation at the endoplasmic reticulum or unfolded protein response pathway plays an important role in ecto-calreticulin translocation (Garg et al. 2010; Garg et al. 2013). Calreticulin translocation pathway is dependent on the inducer signal (Krysko et al. 2012). Ecto-calreticulin can be uptaken by phagocytes and professional antigen presenting cells (APC) through CD91 (Garg et al. 2010). Unfortunately, ecto-calreticulin driven tumor antigen uptake alone is not sufficient for antitumor immune response (Ladoire et al. 2013).

Heat shock proteins are a family of conserved chaperones induced by cell stress including oxidative stress, irradiation, chemotherapeutic drugs, heat and electromagnetic field (Robert 2003; Blank et al. 2009; Horvath et al. 2010). Tumors frequently show elevated Hsp70 levels (Multhoff et al. 2011). In the cytoplasm, overexpressed Hsp70 can inhibit apoptosis and act as a cytoprotector (Horvath et al. 2010) maintaining protein homeostasis (Gehrmann et al. 2008). However, treatments using oxaliplatin, γ-radiation, anthracyclines, epidermal growth factor receptor specific antibody or hypericin based photodynamic therapy can trigger the cell membrane accumulation of heat shock proteins leading to ICD (Gehrmann et al. 2008; Garg et al. 2010; Krysko et al. 2012; Kroemer et al. 2013). On the other hand, cell membrane Hsp70 was also linked with the protection of membrane integrity under stress conditions (Horvath et al. 2010). Therefore, in tumor therapy, cell surface Hsp70 positivity has been associated both with negative prognosis, e.g. in lower rectal carcinomas and in squamous cell carcinoma of the lung (Pfister et al. 2007; Gehrmann et al. 2008) and also with improved outcome e.g. in gastric and colon carcinomas (Pfister et al. 2007). Unfortunately, it is not known how the membrane bound Heat shock proteins can translocate to the cell membrane from the cytoplasm (D'Eliseo et al. 2013) but it was suggested that membrane bound Hsp is associated with

phosphatidilserin in tumor cells and by a flip-flop mechanism, it can be exposed to the outer membrane leaflet into lipid rafts (Multhoff 2007). Heat shock proteins may have a crucial effect on initiating immune response on APCs and NK cells (Gehrmann et al. 2008; Garg et al. 2010). However, heat shock proteins alone on the cell surface are not enough for signaling immunostimulation, they have to form a complex in the cell membrane with a tumor peptide. This happens in paralel with the programmed cell death signaling (Gehrmann et al. 2008; Garg et al. 2010; Multhoff et al. 2011). Besides the immunogenicity of cell membrane Hsp70 (Gehrmann et al. 2008), extracellular heat shock proteins can directly boost the innate immune response (Multhoff et al. 2011).

Both intracellular Hsp70 and Hsp90 assist in protein folding, by stabilizing proteins and preventing their degradation (Calderwood 2013). Membrane exposure of Hsp90 can be induced by bortezomib, anti-EGFR antibody (7A7) and hypericin-based photodynamic therapy (Garg et al. 2013). The surface exposure of Hsp90 may trigger DC activation signal required for cell-cell interaction between dying tumor cell and DC (Spisek et al. 2007), although the Hsp90 receptor on DC remains unknown (Garg et al. 2013).

Release of HMGB1 represents a late signal of ICD with diverse roles. In the nucleus it acts as a non-histone chromatin binding protein interacting with the minor groove of DNA and regulatory molecules such as p53, NF-κB and steroid hormone receptors (Kepp et al. 2011; Guo et al. 2013; Ladoire et al. 2013). Upon cell stress HMGB1 is released either from necrotic or apoptotic cells (D'Eliseo et al. 2013). Extracellular HMGB1 can be a cytokine-like activator of macrophages, a chemotactant for neutrophils and a promoter of dendritic cell (DC) maturation (Guo et al. 2013). However, epigenetic and posttranslational modifications dictate HMGB1 further functions, its acethylation and phosphorilation on both nuclear localization signal leads to secretion to the cytpolasm. Hyperphosphorylation also relocates HMGB1 to the cytoplasm. HMGB1 may be oxidized in a caspase dependent manner or related to ROS production (Guo et al. 2013). The reduced HMGB1 usually binds to RAGE attenuating the pro-inflammatory activity but the oxidized protein binds to toll like receptor (TLR) 2/4 on the dendritic cells which may lead to tumor-specific immune response (Guo et al. 2013). However, if HMGB1 binds to TIM3 (T-cell immunoglobulin

domain and mucin domain 3) on tumor associated dendritic cells, it will inhibit anti-tumor activity (Guo et al. 2013).

These DAMP signals combined with cancer antigens can stimulate the maturation of antigen presenting cells, which finally ‘cross-prime’ and activate anti-tumor T-cell immunity (Kepp et al. 2011; Sachamitr et al. 2012).

As a summary, the altered bioelectrodynamic properties of cancer can result in the enrichment of electromagnetic field in the malignant compared to the normal tissues. Since mEHT, a form of hyperthermic therapy, uses electric field in the radiofrequency range (13.56 MHz) it can target the tumor tissue. The treatment related tumor cell death may occur in a programmed manner utilizing caspase dependent apoptosis, caspase independent apoptosis, programmed necrosis, autophagic cell death or accidental necrosis in the tumor tissue. Heat by itself can induce caspase dependent programmed cell death, autophagic cell death and accidental necrosis. In line with the treatment induced programmed cell death specific DAMP signals may appear on malignant cells which can potentially trigger specific anti-tumor immune response through DCs.

DOI:10.14753/SE.2015.1802

4. OBJECTIVES

1. Determining tumor cell damage induced by a single shot of modulated electrohyperthermia (mEHT) treatment in an *in vivo* xenograft model set up using HT29, an aggressive colorectal cancer cell line, in Balb/c (nu/nu) immunocompromised mice.

2. Investigating the molecular background of cell death induced by the mEHT treatment in the HT29 xenograft model.

3. Characterizing additional, cell stress related molecular changes induced by mEHT in the HT29 xenograft model, which may promote antitumor immune response. Testing for damage associated molecular pattern (DAMP) sequence relevant to immunogenic cell death (ICD) response.

DOI:10.14753/SE.2015.1802

5. MATERIALS AND METHODS

5.1.Tumor model

HT29 colorectal adenocarcinoma cell line xenografted to Balb/c (nu/nu) mice were used to determine the molecular mechanism of cell damage induced by a single shot mEHT treatment.

5.1.1. Cell line

HT29 invasive colorectal adenocarcinoma cell line was propagated in Dulbecco's modified Eagle's minimal essential medium (DMEM)+ GlutaMax, high-glucose (4.5 g/l) medium including 10% heat inactivated fetal calf serum (FCS) and 1% streptomycin-penicillin (5000 units penicillin and 5 mg streptomycin/ml). Cells were released from a sub-confluent monolayer using 0.25% trypsin and 0.22 mg/ml ethylenediaminetetraacetic acid (EDTA) for 5 min and suspended in a serum free medium to reach the required 10^7/ml cell concentration. All reagents were from GIBCO (Invitrogen, Carlsbad, USA).

5.1.2. Animal model

Female nude Balb/c (nu/nu) mice (provided by the Experimental Animal House of the National Research Institute for Radiobiology and Radiohygiene, Budapest, Hungary) maintained in sterile environment, kept on sterilized food and water *ad libitum* under 12 h dark/12 h light cycles. Both femoral regions of 6 to 8-week old mice were subcutaneously injected with 0.1 ml suspension of 10^7/ml HT29 cells. The animals were treated using mEHT 18 days after HT29 cell injection, when the diameter of symmetrical tumor implants had reached ~1.5 cm. Laboratory animals were kept and treated in compliance with the Hungarian Laws No. XXVIII/1998 and LXVII/2002 on the protection and welfare of animals, and the animal welfare regulations of the European Union. The Governmental Ethical Committee approved the study under No. 22.1/609/001/2010.

5.2.Treatment conditions and sampling

Tumor implants in the right legs of Balb/c (nu/nu) mice were placed into the plan-parallel electric condenser of the circuit. The circuit's impedance was kept at a standard 50 Ohm and the electrode arrangement was asymmetrical. Animals were laid down on the rectangular grounded (lower) electrode made of polished aluminum of 72.0 cm^2, which was kept at 37 °C during the treatment. A 2,5 cm^2 round shaped electrode, made of flexible textile (copper-silver-tin coated woven fabric; Lorix Ltd. Bajna, Hungary), was overlaid on the tumor region for full skin contact and cooled from the outside using a wet pad (**Figure 2**). Electromagnetic field was generated at 13.56 MHz radiofrequency using 1/f amplitude modulation by a LabEHY instrument (both from Oncotherm Ltd, Paty, Hungary).

Treatment groups involved 33 animals, which were delivered a single shot of mEHT for 30 min at an average power of 4 W under 100 mg/kg Ketamine and 10 mg/kg Xylazine anesthesia. Parameters were adjusted to keep intratumoral temperature between 41-42 °C on the treated side (right leg), measured with optical sensors (Luxtron FOT Lab Kit, LumaSense Technologies, Inc. CA, USA). The subcutaneous temperature underneath the electrode was kept at ~40 °C and the rectal and the contralateral (untreated) tumor (left leg) core temperature was at ~37 °C. Sampling was made from both, treated (right leg) and untreated (left leg) sides 0, 1, 4, 8, 14, 24, 48, 72, 120, 168, and 216 h after treatment using 3 mice in each group. Additional 5 sham treated control animals were sacrificed 3 at 24 h and 2 at 72 h post-treatment. All in all 38 mice were sacrificed resulting in 76 tumor samples.

One half of the excised tumors was fixed in 10% formalin, dehydrated and embedded routinely into paraffin wax (FFPE). The other half was fresh-frozen in liquid nitrogen and kept at -80 °C in deep freezer until further testing.

DOI:10.14753/SE.2015.1802

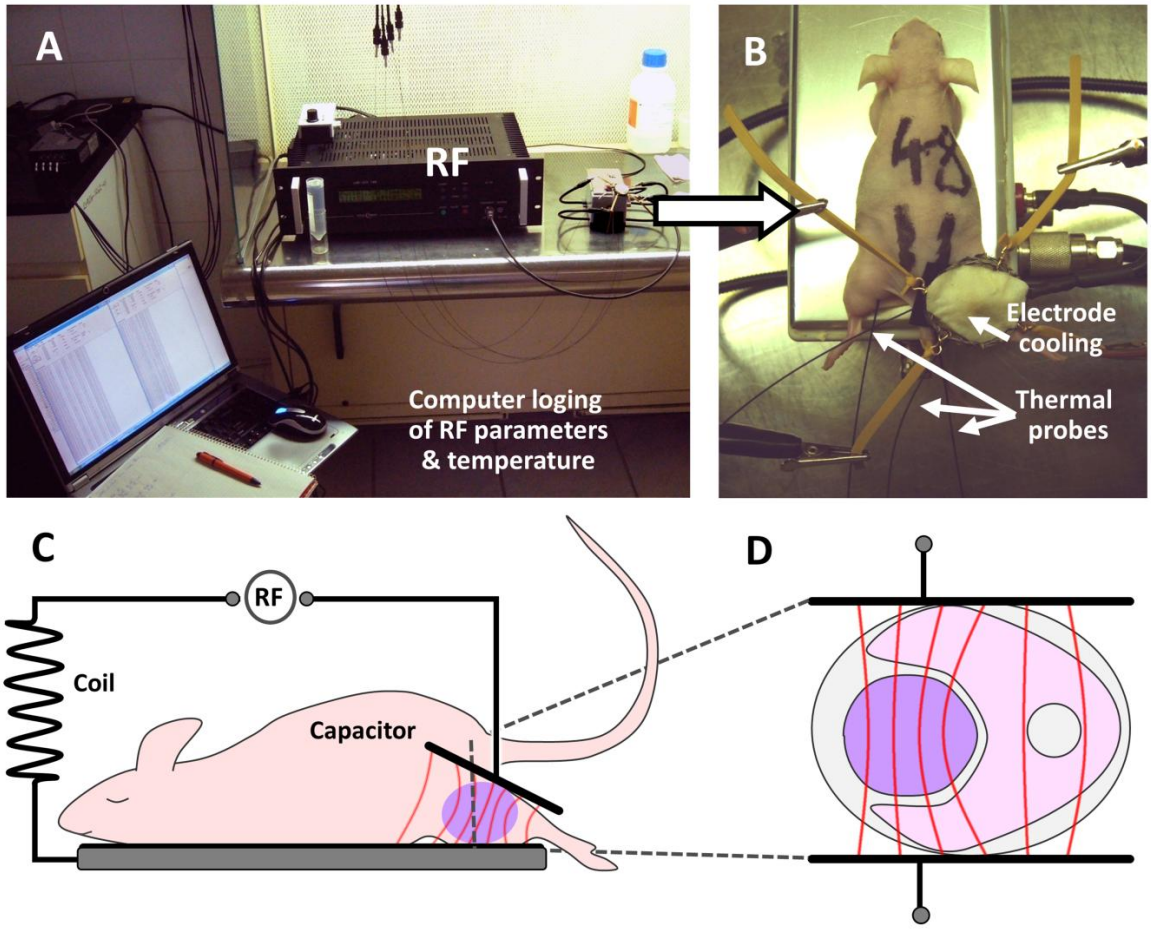

Figure 2 Experimental setup of modulated electrohyperthermia (mEHT) treatment. **A**) Parameters of the electric field and tumor temperature between 41-42 ^{o}C during treatment are monitored. **B**) Thermal probes and electrode cooling of the treated right side. **C-D**) The electric field (red lines) is concentrated in the tumor implant (violet lump) between the condenser electrodes but cannot pass through cell membranes.

5.3. Histomorphological analysis

Whole cross sections from each (11) time point of all 76 (treated, untreated and sham treated control) tumor samples were stained for hematoxylin and eosin (H&E) for histomorphological analysis of signs of cell death. The stained slides were digitalized using Pannoramic Scan and analyzed with the HistoQuant module of Pannoramic Viewer software (all from 3DHISTECH, Budapest, Hungary) based on image color and intensity segmentation. The mEHT related tumor destruction ratio (TDR) was calculated by dividing

the area of destructed tumor tissue (D) by the whole tumor area (W) measured in whole cross sections. Treatment related tumor destruction efficiency (TDE) was assessed by dividing the TDR of the treated by the TDR of the untreated tumor of the same animal (**Figure 3A**). For statistical analysis the Kruskal-Wallis test of the SPSS Statistics v.20 software (IBM Corp. New York, NY) was used.

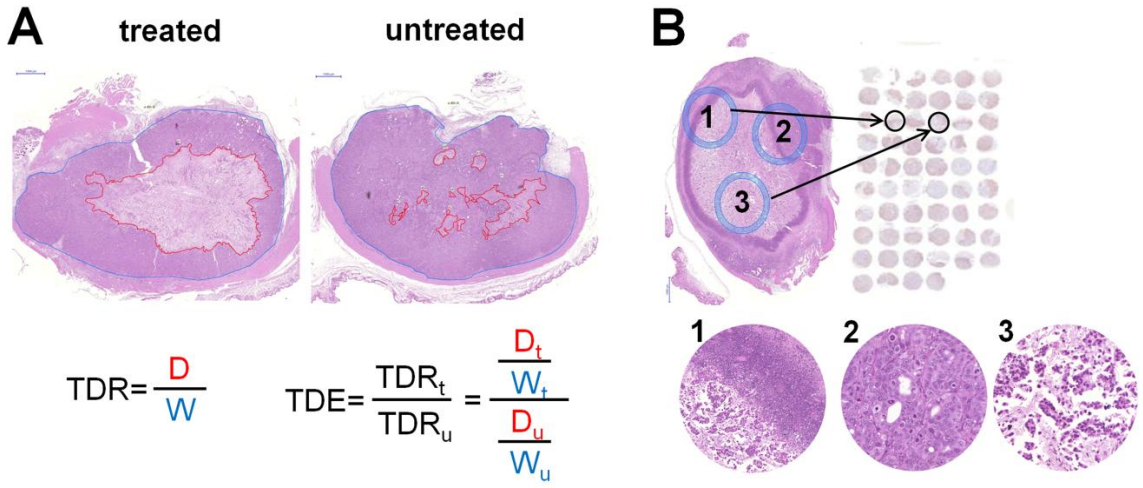

Figure 3 Histomorphological analysis and TMA core selection. A) The damaged tumor areas (circled in red) and the whole tumor areas (circled in blue) were delineated precisely in digital slides at high microscopic power (at x45 theoretical objective magnification) and measured with software. The tumor destruction ratio (TDR) value was calculated by dividing the area of destructed tumor tissue (D in red) by the whole tumor area (W in blue) measured in cross sections both of the treated (t) and untreated (u) tumors. The tumor destruction efficiency (TDE) of mEHT treatment was assessed by dividing the TDR of the treated tumor by the TDR of the untreated tumor of the same mouse. **B**) Standard regions of 2 mm diameter from the damaged-intact tumor border (1 and 2) and from the damaged tumor center (3) were selected based on H&E stained slides.

The number of apoptotic bodies was counted at x100 objective magnification in 10 different microscopic fields of views (FOV) of 3 treated and 3 untreated samples at 48, 72 h post-treatment time points. Statistical analysis was carried out using SPSS Statistics v.20 software (IBM Corp).First the normality distribution of the data was tested by Sapiro Wilk test followed by a Student t-test.

In the course of the morphological analysis the signs of apoptotic, necrotic and autophagic cell death were taken into consideration.

5.4. Molecular analysis

To assess the early (4 h post-treatment) mRNA based molecular changes of the mEHT induced tumor damage a human genome expression array was used. To determine the form of cell death and the stress related tumor response first as a screening method an apoptosis array was applied followed by verifying the molecular changes using immunohistochemistry, immunofluorescence, TUNEL assay and western blot.

5.4.1. mRNA chip analysis

To determine the early treatment related mRNA changes mRNA chip analysis was carried out in 9 tumor samples.

5.4.1.1.Total RNA isolation and RNA quality control

Frozen tissue sections were prepared both from the 3 treated and the 3 untreated samples collected at 4 h post-treatment and from the 24 h 3 sham treated controls. Total RNA was extracted by Roche MagNA Pure LC RNA Isolation Tissue Kit (Roche, Basel, Switzerland). RNA concentration was measured by NanoDrop instrument (Thermo Scientific, Rockford, IL, USA). The quality of the nucleic acid was determined with microcapillary electrophoresis system using Agilent BioAnalyzer 6000 Pico LabChip kit (Aligent Technologies, Santa Clara, CA, USA). With RNA Integrity Number above 7 (RIN > 7) 100 ng total RNA from each sample were mixed and 250 ng pooled total RNA was amplified and labeled in each group.

5.4.1.2.Microarray analysis

The recommendation of Minimum Information About a Microarray Experiment (MIAME) guideline was followed (Brazma et al. 2001). Amplification and labeling of the transcripts was performed by using Affymetrix 3’ IVT Express Kit (Affymetrix, Santa Clara, CA, USA). Samples were hybridized on HGU133 Plus2.0 arrays (Affymetrix) at 45 °C for 16 h. The microarrays were washed and stained on Fluidics Station 450 device (Affymetrix) using the vendors kit with the FS450_001 wash protocol. Fluorescent signals were detected

by Gene Chip Scanner 3000 (Affymetrix) following the antibody-based signal amplification with streptavidin-phycoerythrin according to manufacturer's instructions.
From the CEL files quality control and RNA digestion plots were generated in R-environment using the Bioconductor system. The differentially expressed genes between the analyzed sample groups were determined by SAM (Significance Analysis of Microarrays) at the significance level $p < 0.05$. Feature selections were done according to the log2FC (log2 fold change) values to select at least two-fold up/downregulated genes.

5.4.2. Apoptosis protein array

To screen the apoptosis related protein changes, tissue lysates were prepared from the whole tumor sections of the 8, 14 and 24 h treated and 24 h sham treated control samples. Proteins were isolated from the frozen samples using extraction buffer (20 mM Tris, 2 mM EDTA, 150 mM NaCl, 1% Triton-X100, 10 µl/ml phosphatase inhibitor and 5 µl/ml proteinase inhibitors) for 30 min on ice, followed by centrifugation at 15,000 rpm at 4 °C for 15 min. Protein concentration was measured with Bradford assay the lysates protein concentration was set to 100 µg/µl. The expression of 35 apoptosis-related proteins was tested simultaneously in the treated and untreated samples using a nitrocellulose membrane Proteome Profiler ^{TM} Human Apoptosis Array Kit array (R&D, Minneapolis, MN). Arrays were incubated on a shaker with 250 µl of 1,200 µg/ml protein lysates at 4 °C overnight, then with biotinylated anti-human IgG for 60 min and Streptavidin-horseradish peroxidase (HRP) conjugate for 30 min and visualized using a chemilunescence (ECL) kit (SuperSignal® West Pico Chemiluminescent Kit; Thermo Sci., Rockford, IL) for 10 min in Kodak Image Station 4000 mm (Rochester, NY). Semi-quantitative analysis of signal density was done using ImageJ 1.45s (http://rsbweb.nih.gov/ij/).

5.4.3. Immunohistochemistry and immunofluorescence

All 76 FFPE tissue samples were used for creating tissue microarray (TMA) blocks to further characterize the proteins –and their subcellular distribution- related to mEHT induced cell death and cellular stress. TMAs included 3 cores of 2 mm diameter from, 2 from the edges of degraded and intact tumor border and 1 from the degraded center, of each

archived tissue using the semi-automated TMA Master (3DHISTECH Ltd., Budapest, Hungary) (**Figure 3B**). For immunohistochemistry 4 μm thick sections were dewaxed and rehydrated routinely, and then endogen peroxidase enzymes were blocked using 3% hydrogen peroxide in methanol for 20 min except for immunfuorescence. Antigen retrieval was performed either in electric pressure cooker (Avair Ida YDB50-90D, Biatlon kft, Pécs) at ~105°C for 50 min or in a microwave oven (Whirlpool, Benton Harbor, MI) ~100^{o}C for 40 min by using buffer made either of 0.01 M sodium citrate-citric acid (citrate, pH 6.0) or 0.1 M Trisbase and 0.01 M EDTA (T-E, pH 9.0). For blocking non-specific tissue binding of antibodies a buffer containing 1% bovine serum albumin (BSA) and 0.1% sodium azide (Sigma Aldrich, St Luis, MO) was used for 20 min. Then, sections were incubated in humidity chambers at room temperature for 16 h using the primary antibodies listed in **Table 1**. For immunohistochemistry the EnVision polymer peroxidase detection system (DAKO) was used for 30 min followed by enzyme development for 5-8 min under microscopic control using either 3,3'-diaminobenzidine (DAB, brown) kit (RE7105, Leica-NovoCastra, Newcastle, UK) or aminoethylcarbazole (AEC, red) kit (Dako, K3461). For immunofluorescence detection either Alexa546 (orange-red) or Alexa488 (green, both from Invitrogen-Molecular Probes) anti-rabbit Ig-s diluted in 1:200 were used for 90 min. Between incubations the slides were washed in Tris-buffered saline (TBS) buffer for 3x2 min and finally counterstained using hematoxylin or 4',6-diamidino-2-phenylindole (DAPI, Invitrogen-Molecular Probes). For membrane staining wheat germ agglutinin conjugated with Alexa488 (WGA, Invitrogen-Molecular Probes) was used.

Biomarker expression revealed by immunofluorescence was evaluated using image (color, intensity and size) segmentation based software HistoQuant (3DHISTECH). 3-5 representative annotations per tumor section involving >1000 cells each were tested. Relative mask area (rMA) was calculated by dividing stained area with the whole annotation area in the following reactions: Bax, cleaved caspasase 3, TRAIL-R2, HMGB1, Hsp70 and Hsp90. In the rest of detected markers, nuclear, mitochondrial or cell membrane signals were counted in 10 (FOV) in each core at x100 magnification. Analyzing a single time point, normality of the data was tested by Sapiro-Wilk test than in case of normal distribution the Student t-test (independent) was applied, in case of non-normal distribution

the Mann-Whitney U-test was used. To analyze time series, we used the Friedmann test followed by the Wilcoxon post-hoc test. The results were significant at $p < 0.05$. For all statistical analysis the SPSS software (SPSS Statistics v.20; IBM, New York, NY) was used.

Table 1. Antibodies and conditions used for immunohistochemistry and immuno-fluorescence.

Antigen	Clonality	Host	Dilution	Vendor	Antigen retrival
AIF	polyclonal	rabbit	1:25	Cell Signaling	T-E
Bax	polyclonal	rabbit	1:50	Sigma Aldrich	T-E
cleaved caspase-3	polyclonal	rabbit	1:100	Cell Signaling	citrate
cytochrome c	polyclonal	rabbit	1:50	Cell Signaling	T-E
mitochondrial antigen	monoclonal (113-1)	mouse	1:50	BioGenex Laboratories	T-E
RIP1	monoclonal (D94C12)	rabbit	1:100	Cell Signaling	T-E
RIP3	polyclonal	rabbit	1:400	Sigma Aldrich	T-E
TRAIL-R2	monoclonal (D4E9)	rabbit	1:50	Cell Signaling	T-E
Ki-67	monoclonal (SP6)	rabbit	1:600	LabVision	T-E
calreticulin	polyclonal	rabbit	1:100	Cell Signaling	T-E
HMGB1	polyclonal	rabbit	1:200	Cell Signaling	T-E
Hsp70	polyclonal	rabbit	1:50	Cell Signaling	T-E
Hsp90	polyclonal	rabbit	1:100	Cell Signaling	T-E
CD3	polyclonal	rabbit	1:2	DAKO	T-E
MPO	polyclonal	rabbit	1:200	Sigma Aldrich	citrate

Vendor specification: Sigma Aldrich, ST Luis, MO; Cell Signaling, Danvers, MA; LabVision Thermo Sci, Rockford, IL; BioGenex Laboratories, San Ramon, CA.

5.4.4. Terminal deoxynucleotidyl transferase nick end labeling (TUNEL) assay

TUNEL assay was used to pre-screen FFPE TMA sections for DNA fragmentation including the whole time-lapse series of mEHT treated, untreated and sham treated control xenografts. Based on the semi-quantitative results the assay was also performed on whole cross sections of mEHT treated tumors and their matched untreated pairs of 24h and 48h post-treatment. TUNEL assay is based on the detection of DNA nick ends by terminal deoxynucleotidyl transferase (TdT) and linking them with fluorochome labeled deoxyuridine triphosphate (dUTP) nucleotides by the TdT enzyme. Labeling in cell nuclei is proportional to the amount of fragmented DNA as a result of programmed cell death. The "Click it TUNEL Alexa Fluor 488 Imaging Assay" (Invitrogen) was used according to the manufacturer's instructions. Briefly, dewaxed and rehydrated slides were heated in a citrate based pH 6.0 antigen unmasking solution (H-3300, Vector Lab, Burlingame, CA) using electric pressure cooker (Avair Ida, as above). Then slides were incubated at 37 °C for 60 min with a cocktail of alkyne substituted dUTP and TdT followed by the fluorochrome for 30 min at room temperature which is coupled to dUTP under copper (I) catalysis. Finally, nuclear DNA was stained with DAPI (see above). The number of biomarker positive cells was counted at x100 objective magnification in 10 different microscopic FOV of 3 treated and 3 untreated samples at each tested time point. DAPI co-staining was used for confirming the critical nuclear localization in the samples. The data was first tested by Kolmogorov-Smirnov normality test followed by the independent t-test (SPSS Statistics v.20; IBM, New York, NY).

5.4.5. Western blot

Tissue lysates were prepared from 4, 14 and 24 h treated, untreated and 24 h sham treated control frozen samples to measure expression of proteins characteristic to programmed cell death. Extraction buffer (20 mM Tris, 2 mM EDTA, 150 mM NaCl, 1% Triton-X100, 10 µl/ml phosphatase inhibitor and 5 µl/ml proteinase inhibitors) for 30 min on ice were used to produce tissue lysates, followed by centrifugation at 15,000 rpm at 4 °C for 15 min. Protein concentration was measured with Bradford assay. The extracts were mixed with 5x

Laemmli sample buffer containing 5% 2-mercaptoethanol and heated to 95 °C for 5 min. 30 μg protein was loaded into each well of 12% sodium dodecylsulfate polyacrylamide gel (SDS-PAGE) and electrophoresis was done at 150 V for 1 h. Proteins were then immunoblotted into polyvinylidene difluoride (PVDF) membrane at 75 mA and 4 °C overnight. For immunodetection, membranes were sequentially incubated with 5% semi-skimmed milk as a protein block for 60 min, followed by the incubation with primary antibody (**Table 2**) at 4 °C and (HRP)-conjugated goat anti-rabbit IgG (1:1000; Cell Signaling) for 60 min and SuperSignal ECL kit (Thermo Sci.) for 10 min. For loading control β-actin (1:500, Cell Signaling) was used. The precision Plus Protein Standard ladder produced bands at 250kDa, 150-, 100-, 75-, 50-, and 37kDa. Signals were detected using Kodak Image Station and its 4.1 software. All reagents except where otherwise indicated were from BioRad (Hercules, CA). Semi-quantitative analysis was done using ImageJ 1.45s software (http://rsbweb.nih.gov/ij/).

Table 2. Antibodies and condition used for Western immunoblots

Antigen	Clonality	Host	Dilution	Vendor
caspase-3	polyclonal	rabbit	1:1000	Cell Signaling
caspase-8	polyclonal	rabbit	1:2000	Sigma Aldrich
AIF	polyclonal	rabbit	1:1000	Cell Signaling
RIP1	polyclonal	rabbit	1:1000	Sigma Aldrich

DOI:10.14753/SE.2015.1802

6. RESULTS

6.1. Histomorphological analysis of treatment related tumor cell death

The H&E stained cross sections of HT29 xenografts showed significant damaged central zones of the treated tumors between 24-120 h post-treatment, which were clearly demarcated as pale areas (**Figure 3A**). At this stage we did not discriminate among the different types of cell death subroutines. Free annotation option within the digital slide viewer software allowed accurate area measurements in μm^2. Damaged areas were correlated with the whole tumor area (TDR) (**Figure 4A**). When TDR values of treated and untreated tumors were compared the mEHT related cell destruction (TDE) was not significantly changed within the first 14 h post-treatment but it showed a dynamic increase between 14-24 h. The peak of a single shot treatment showed a 7-fold increase in cell damage 72 h after mEHT treatment (**Figure 4B**), which was gradually reduced between 120 h and 216 h.

H&E slides were lack of any morphological sign of autophagic cell death.

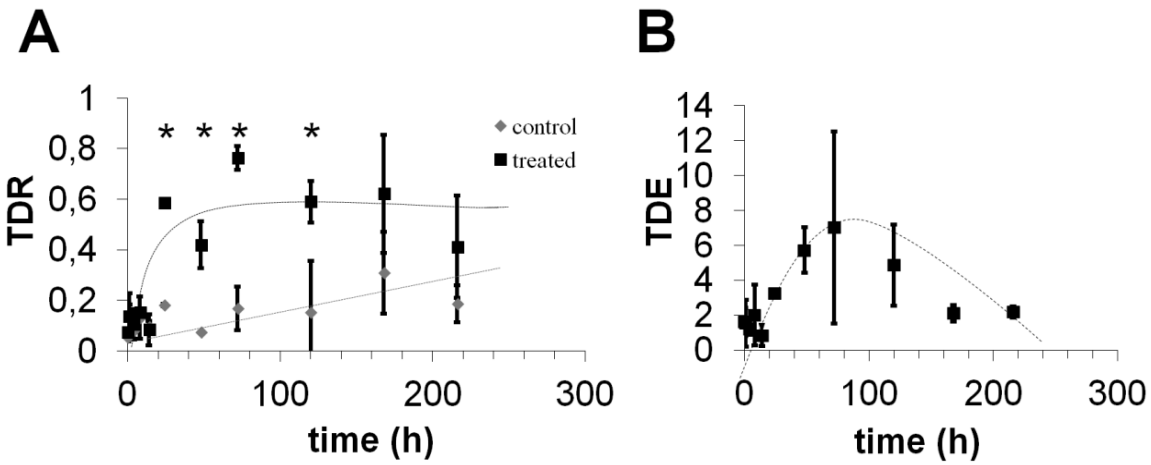

Figure 4. Measurement of mEHT related tumor destruction. A) The TDR (tumor destruction ratio) upon mEHT treatment significantly exceeded that measured in the untreated tumors from 24h post-treatment on. **B**) The TDE (tumor destruction efficiency) values, which exclude the systemic effect of mEHT treatment, also show treatment related increase with a peak at 72 h post-treatment.

6.2. Detection of treatment related DNA fragmentation

TUNEL assay utilizing nick end labeling of damaged and fragmented DNA with fluorescent labeled dUTP was performed in the HT29 xenograft tumors. First, the kinetics of DNA damage was pretested in TMA sections for selecting the most appropriate time points for detailed analysis ($\chi^2(11) = 26.931$, $p < 0.05$). The TUNEL assay proved significantly higher programmed cell death related DNA fragmentation in whole cross sections of the treated compared to the untreated tumors both at 24 h and 48 h post-treatment (**Figure 5A, B**). In agreement with this, there was a significantly higher degree of nuclear shrinking (pycnosis) and accumulation of dense chromatin fragments (apoptotic bodies) in the treated compared to the untreated tumors with a peak difference reached at 72 h, as counted at high power (x100) microscopic fields of H&E stained slides (**Figure 5A, C**).

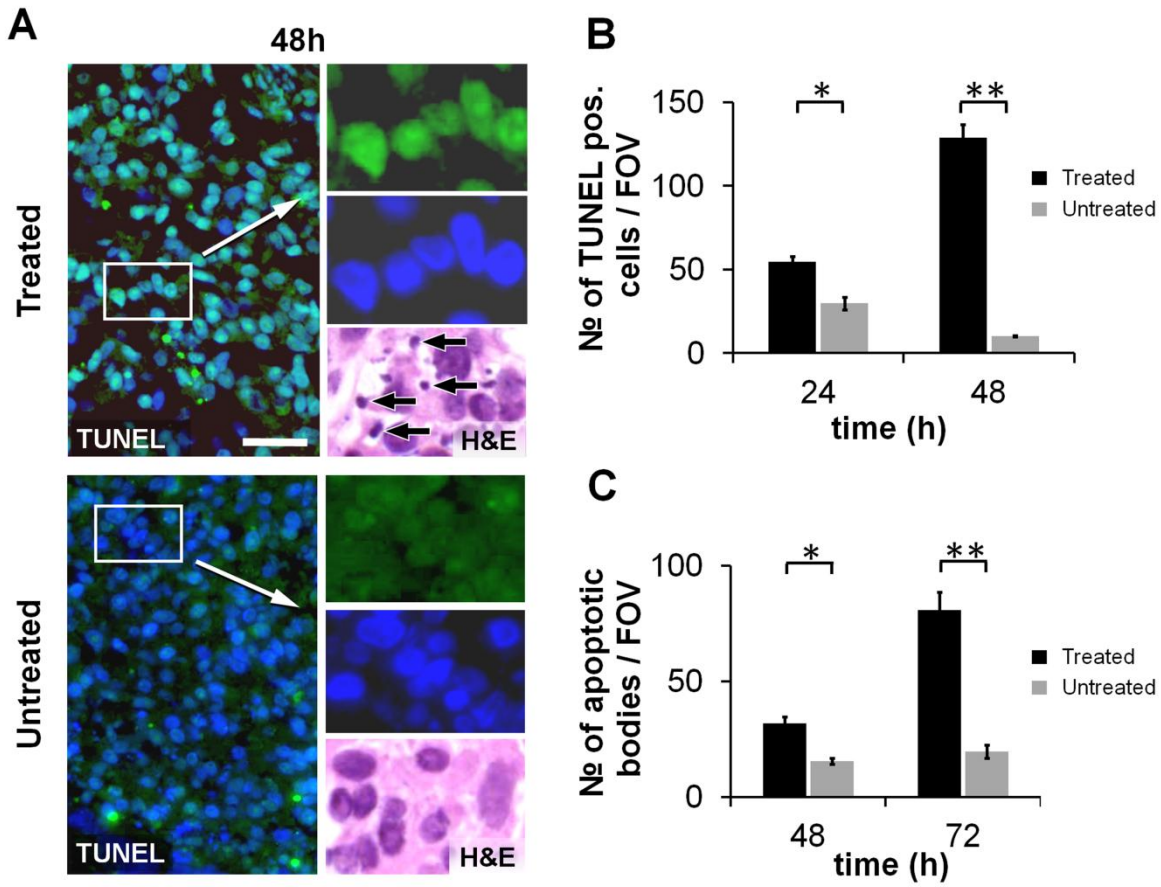

Figure 5 showing DNA fragmentation, nuclear shrinkage and apoptotic bodies. A) Significant elevation of DNA fragmentation revealed by TUNEL assay (green fluorescence), nuclear shrinkage and apoptotic bodies (H&E staining; arrows) in mEHT treated (upper row) compared to untreated tumors (lower row), at 48h post-treatment. Insets show single channel views of areas within rectangles at higher power. TUNEL and DAPI (blue) double positivity verifies nuclear DNA staining in identical cells labeled. Untreated tumor cells show only basic green fluorescence. Bar indicates 50 μm in the left column and 15 μm in the right column. **B**) Graphs showing significantly increased mean number of TUNEL positive cells both at 24 h and 48 h post-treatment (black columns); and **C**) of apoptotic bodies at 48 h and 72 h post-treatment (black columns) compared to the untreated controls (grey columns) (*$p < 0.05$, **$p < 0.01$).

6.3. Detection of treatment related differential mRNA expression

Messenger RNA gene expression was measured from pooled samples of the 4 h treated, 4 h untreated and 24 h sham treated tumors, respectively using Affymetrix HGU133 Plus2.0 mircoarrays. Modulated EHT treatment induced significant up- or down-regulation of 48

transcripts of 39 genes compared to controls. Members of the heat shock protein 70 family including HSPA1A, HSPA1B, HSPA4, HSPA6 and HSPA8, and their co-chaperons hsp40 (DNAJB1 and DNAJB4) and Bag3 became upregulated. Hsp90 alpha (HSP90AA1) and hsp60 (HSPD1) gene transcripts were also elevated upon mEHT treatment (**Figure 6**).

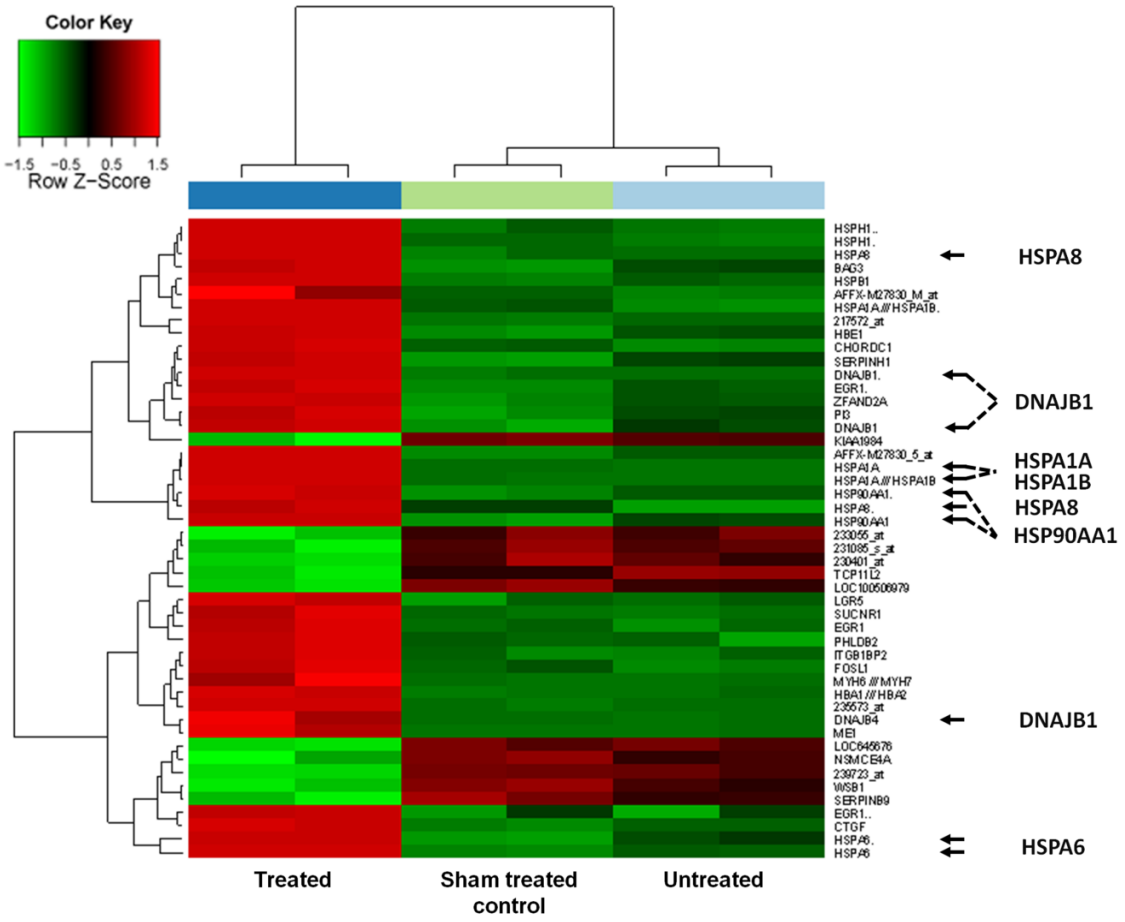

Figure 6. Heat map on gene expression summarizing transcripts showing significantly differential expression 4 h after mEHT treatment of HT29 colon cancer xenografts. Arrows highlight the elevated expression (red boxes) of heat shock protein genes from the Hsp70, Hsp40, Hsp90 and Hsp60 families in the treated samples (left column) compared either to sham treated (middle) and untreated samples (right).

6.4. Detection of apoptosis related differential protein expression

The expression of 35 apoptosis related proteins was compared using pooled samples of 3 animals at each time point from treated (8, 14 and 24 h post-treatment) and sham treated

(24 h post-treatment) experiments on nitrocellulose membrane plotted protein arrays. Protein extraction was made using whole cross sections of the dissected frozen tumors.

We detected the early (8h post-treatment) elevation of 12 apoptosis related proteins including Bax, catalase, c-IAP, cytochrome c, TRAIL-R2, FADD, Hsp60, Hsp70, Hsp27, HTRA2/Omi, HO-2, SMAC/Diablo (**Figure 7**). Due to the cell death related progressive inhomogenity of treated tissues observed at morphological analysis, only the 8 h post-treatment samples were considered representative.

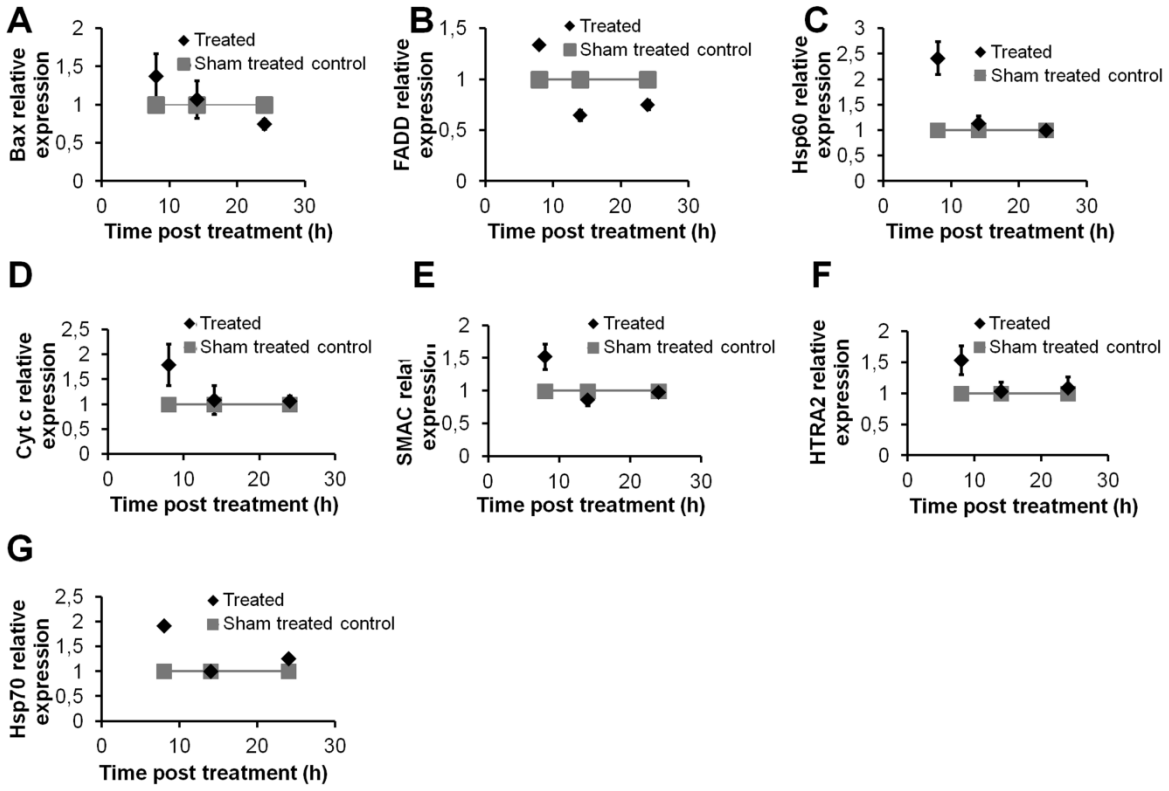

Figure 7. Modulated EHT induced elevated expression of apoptosis related proteins. Elevated expression of **A**) Bax, **B**) FADD, **C**) Hsp60, **D**) cytochrome c, **E**) SMAC/Diablo **F**) HTRA2/Omi and **G**) hsp70 proteins upon mEHT treatment of HT29 xenograft tumors in apoptosis protein arrays.

No significant change in the expression of Bad, pro-Caspase-3 and cleaved Caspase-3 proteins were detected between the treated and the control samples (**Figure 8**)

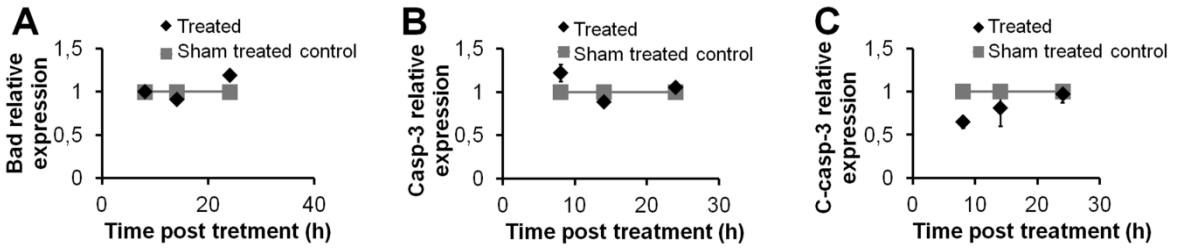

Figure 8. Unchanged expression of apoptosis related proteins upon mEHT. Unchanged expression of **A)** Bad, **B**) procaspase-3 (casp-3) and **C**) cleaved caspase-3 (c-casp-3) proteins upon mEHT treatment of HT29 xenograft tumors in apoptosis protein arrays.

The mEHT treatment resulted in the reduced expression of 5 apoptosis related proteins including Fas, phospho-p53 (S392), phosphor-p53 (S15) Survivin and XIAP. (**Figure 9**)

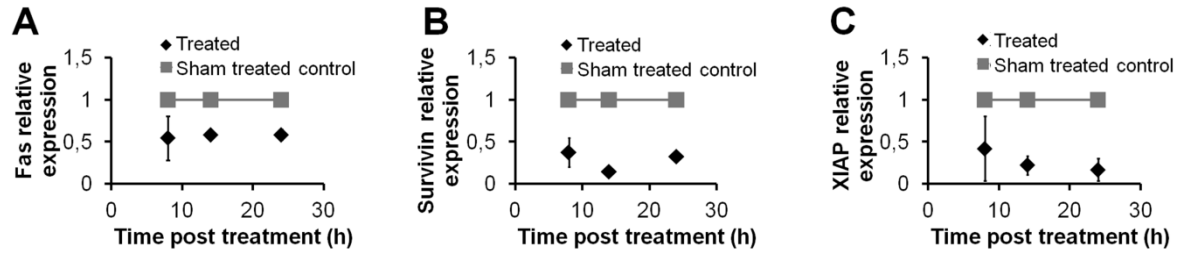

Figure 9. Reduced expression of apoptosis related proteins upon mEHT. Reduced expression of **A**) Fas, **B**) Survivin and **C**) XIAP proteins upon mEHT treatment of HT29 xenograft tumors in apoptosis protein arrays.

No signal was detected in case of the following proteins: BAD, Bcl-2, Bcl-x, cIAP2, claspin, clusterin, TRAIL-R1, Hif-1a, HO1, Livin, PON2, p21, p53(S46), pRad17 and TNFRSF1A.

The expression and subcellular localization of Bax, cleaved Caspase-3, cytochrome c, TRAIL-R2 and Hsp70 proteins were further tested *in situ* in tissue sections using immunohistochemistry or immunofluorescence technique.

6.5. Detection of treatment related differential protein expression *in situ*

6.5.1. Programmed cell death related proteins

TMA sections prepared from HT29 xenograft tumor samples were immunostained using antibodies recognizing the following programmed cell death and proliferation related protein antigens: AIF, Bax, cleaved Caspase-3, Cytochrome c, RIP1, RIP3, TRAIL-R2 and Ki67.

Modulated EHT treatment resulted in the significant mitochondrial accumulation of Bax protein and the mitochondrial to cytoplasmic release of cytochrome c protein both at 8 h ($*p < 0.05$) and 14 h ($**p < 0.01$) post-treatment. Mitochondrial localization of these pro-apoptotic proteins was confirmed using double immunofluorescence staining for either of these proteins and anti-mitochondrial antigen (**Figure 10**).

Treatment related significant cytoplasmic to nuclear translocation of the AIF protein was observed both at 14 h ($*p < 0.05$) and 24 h ($**p < 0.01$) post-treatment (**Figure 11A, B**) as an effector for DNA fragmentation. As opposed to this, normal cytoplasmic granular (mitochondrial) expression of AIF was seen in the intact tumor cells and in cells of the reactive microenvironment. Also AIF western immunoblots confirmed the mitochondrial 62 kDa band in both treated and untreated samples and the 57 kDa band corresponding to the molecular range of released protein from the mitochondria in the treated samples 14 h post-treatment (**Figure 11C**).

Though a significant elevation in the effector cleaved Caspase-3 levels was observed in the mEHT treated tumors compared to their untreated controls ($*p < 0.05$) at 4 and 8 h post-treatment, the signals were detected only at a very low level resulting in an undetectable global difference in Western immunoblots between treated and control samples. Furthermore, the cleaved Caspase-3 reaction was almost exclusively localised to inflammatory cells involving myeloperoxidase positive neutrophil granulocytes (monocytes) and CD3 positive immature T lymphocytes demarcating the cleaved Caspase-3 negative tumor nests (**Figure 12**).

DOI:10.14753/SE.2015.1802

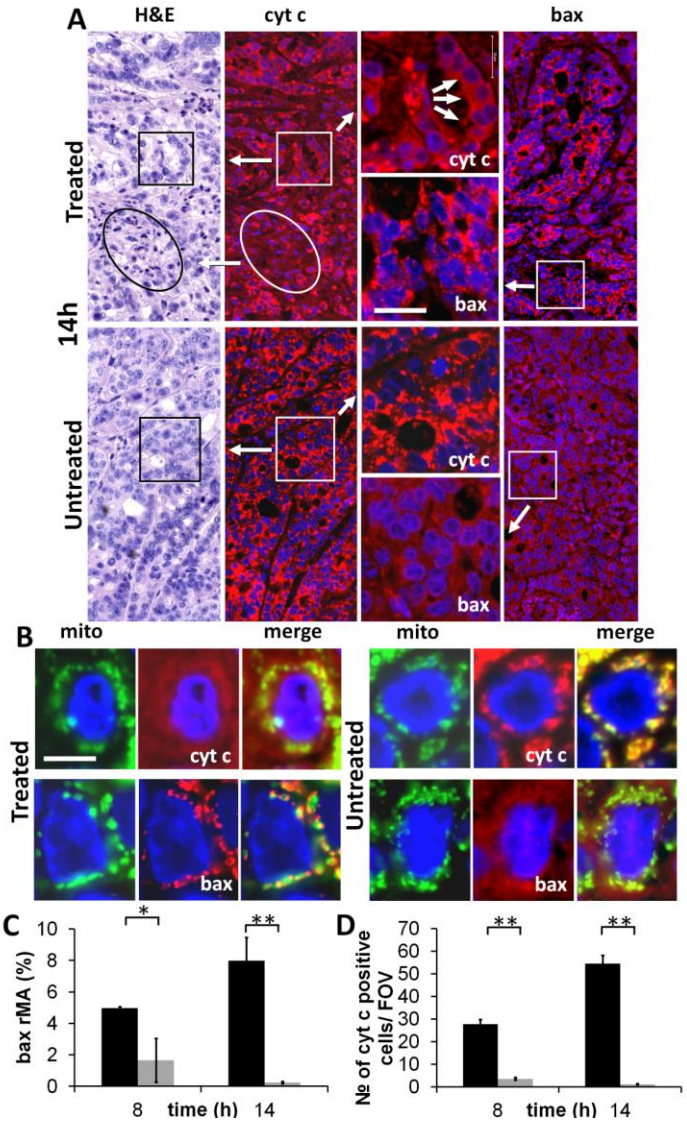

Figure 10. Immunofluorescence staining (Alexa 564, red) for the pro-apoptotic Bax and cytochrome c (cyt c) proteins and semi quantitative image analysis of the signals in mEHT treated and untreated tumors. A) Mitochondrial accumulation of Bax and cytoplasmic release of cytochrome c (cyt c) are linked with the mEHT treatment at 14 h. Insets highlight areas in rectangles at high power (arrows, x100) where cytoplasmic delocalization of cyt c in the treated tumor is shown by arrows. Cell nuclei are stained using DAPI (blue). Identical sections labeled for cyt c were later stained also for H&E where circled area reveals pyknotic tumor cell nuclei. **B**) Mitochondrial localization of Bax in the treated and cyt c (both red) in the untreated samples was confirmed by their co-localization with anti-mitochondrial antigen (mito - green). Bar indicates 25 μm in the insets and 60 μm in the rest of 4A and 10μm in 4B. **C**) Graphs showing significant increase of accumulated granular Bax reaction in tumor cells (*$p < 0.05$; **$p < 0.01$) (rMA- relative mask area) and **D**) loss of granular cyt c reaction (black columns) upon mEHT treatment compared to untreated controls (grey columns) (FOV- field of views).

DOI:10.14753/SE.2015.1802

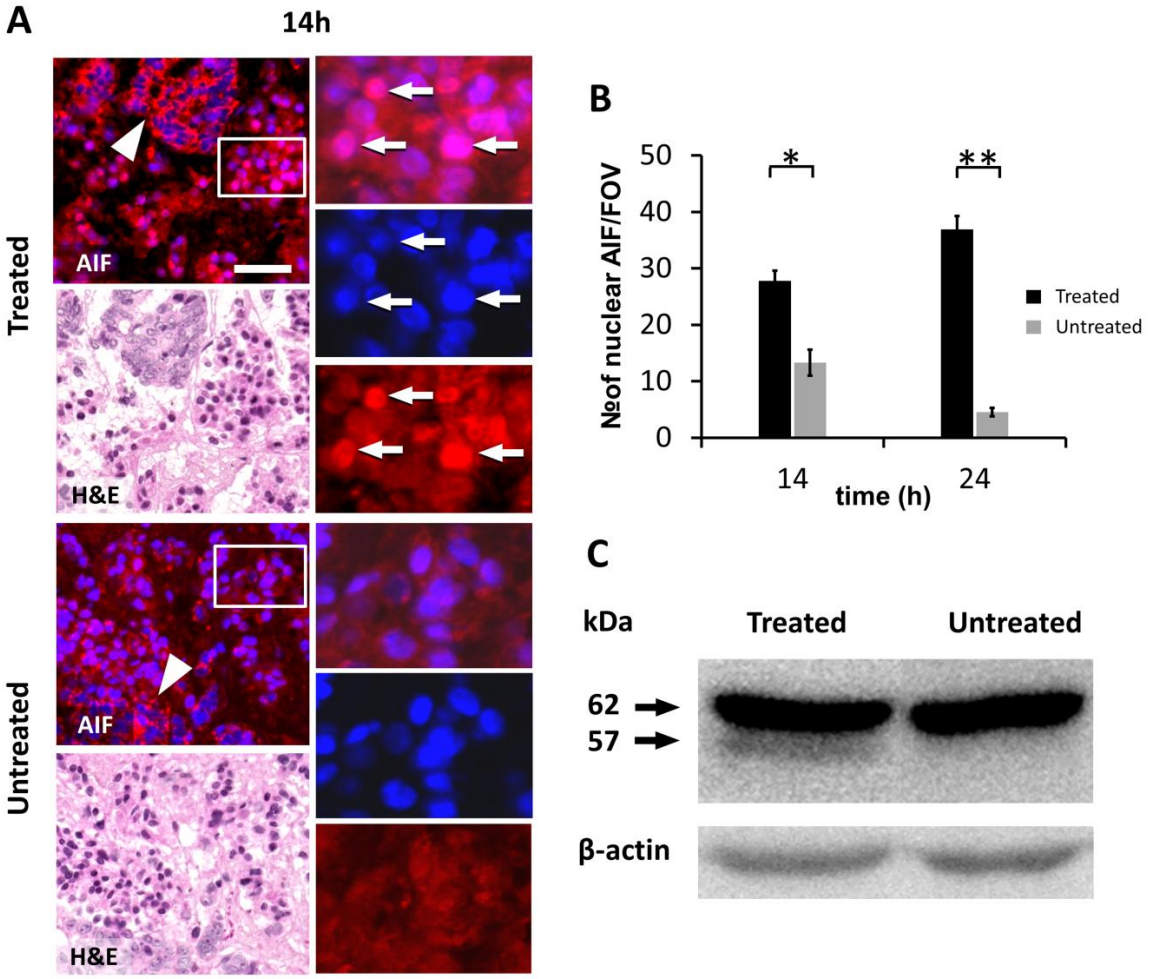

Figure 11. Activation of apoptosis inducing factor (AIF) upon mEHT treatment of HT29 xenografts. A) Identical tissue sections consecutively stained for AIF using immunofluorescence (Alexa 564, red) then with H&E. Many tumor cells show nuclear translocation of AIF in the treated but not in the untreated tumors. Insets show single channel views at higher power of representative areas within rectangles. Arrows highlight identical cells with nuclear AIF staining. Arrowheads points to tumor nests of granular mitochondrial AIF staining characteristic of intact tumor cells. Cell nuclei are stained using DAPI (blue). Bar indicates 50 μm in the left and 25 μm in the right column. **B**) Graph showing the significantly elevated mean number of nuclear AIF positive cells in the treated (black columns) compared to the untreated (grey columns) tumors (*$p < 0.05$; **$p < 0.001$). C) In western immunoblots the 57 kDa cleaved AIF protein is detected only in the treated tumors at 14 h post-treatment besides the mature 62 kDa protein.

DOI:10.14753/SE.2015.1802

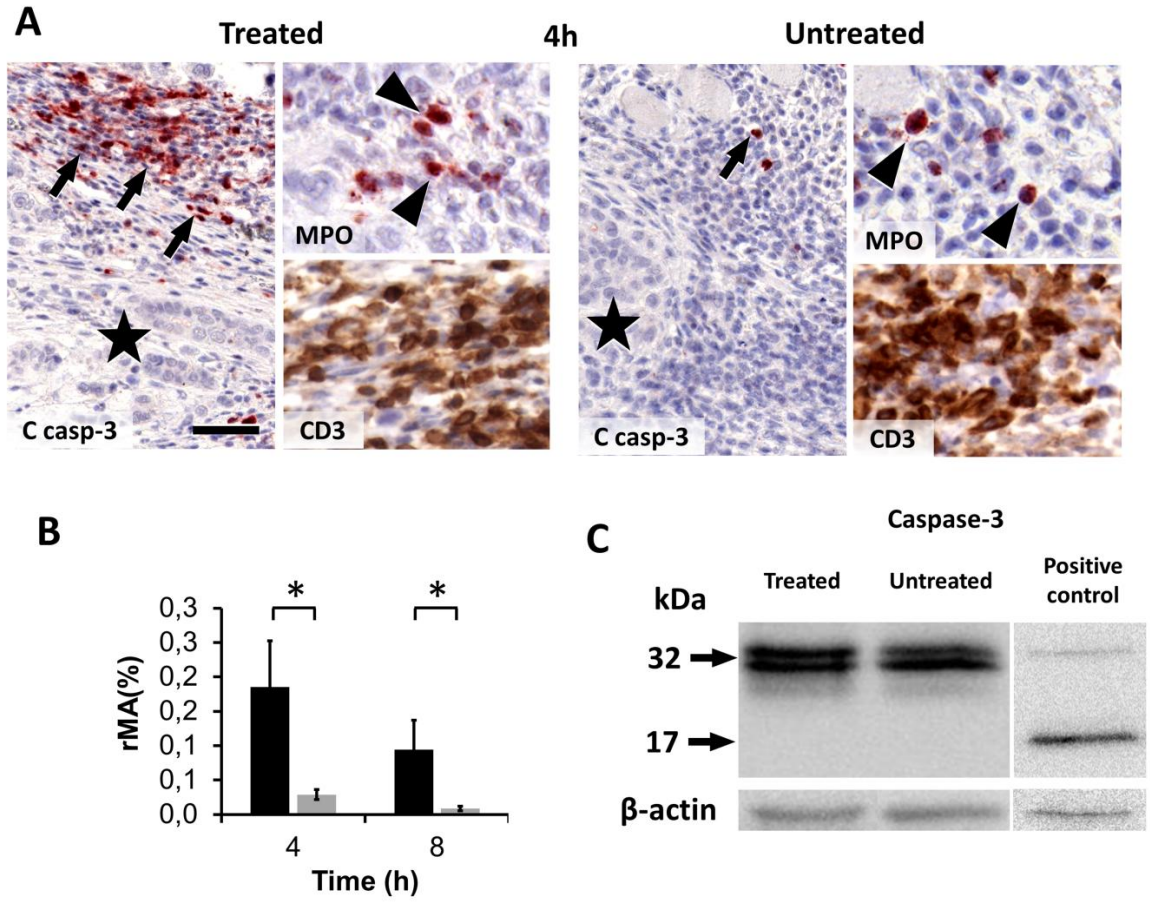

Figure 12. Expression of caspase-3 protein in mEHT treated HT29 xenografts. A) Though treated tumors show significantly more cleaved/activated caspase-3 (C casp-3) positive cells than untreated controls (left column; AEC, red), the reaction is primarily localized to peritumoral leukocytes (arrows) and not to tumor nests (asterisks). Bar indicates 50 μm in the left and 25 μm in the right columns. **B**) Cleaved caspase-3 positive areas (relative mask area; rMA) measured with the HistoQuant software are significantly higher (*$p < 0.05$) in the treated than in the untreated samples both at 4 h and 8 h post-treatment. **C**) Caspase-3 expression (either the full length 32 kDa or the missing 17 kDa cleaved fragment) does not differ significantly in the treated compared to the untreated tumors. The 17 kDa fragment is detected in Staurosporine treated control HTC-116 cell extract.

Based on the apoptosis array results, which revealed an elevated TRAIL-R2 expression in the treated compared to the untreated samples, immunofluorescence staining also showed a highly significant elevation (**$p < 0.01$) of TRAIL-R2 protein levels in the mEHT treated

compared with the control samples both at 8 h and 14 h post-treatment using automated image analysis based on signal intensity segmentation and area measurement (**Figure 13**).

Furthermore, there was no significant change in RIP protein levels (neither in RIP1 nor in RIP3) upon mEHT treatment. RIP kinase could have mediated necroptosis, another caspase independent form of programmed cell death, either using RIP1 or RIP3.

There was no significant change in caspse-8 expression either on immunostaining or on western blot where the cleaved fragment was not detected at any time point.

Ki67 immunostaining also revealed no significant difference in cell proliferation at any time point in the morphologically intact tumor areas between the mEHT treated and control samples, while the staining was lost from 24h post-treatment on in the destructed areas (*data not shown*).

DOI:10.14753/SE.2015.1802

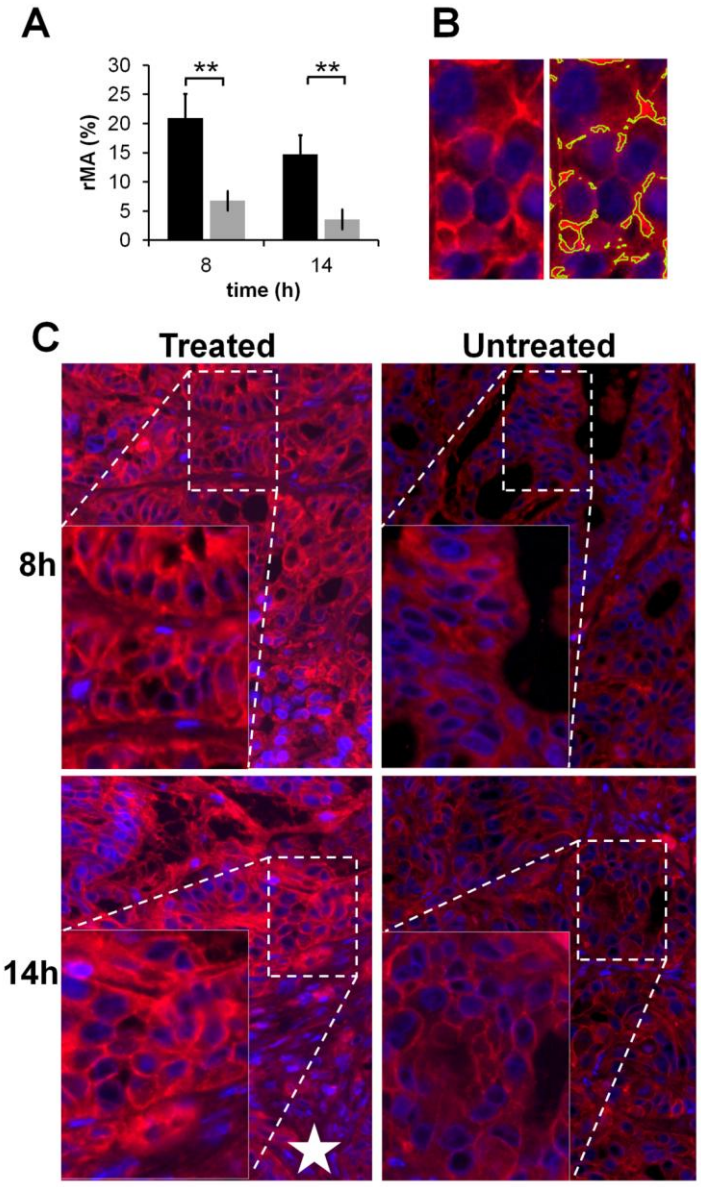

Figure 13. Significant upregulation of TRAIL-R2 cell membrane death receptor upon mEHT treatment of HT29 xenografts. A) Image analysis using the HistoQuant software confirms the significantly elevated expression of TRAIL-R2 protein both 8h and 14h post treatment (black columns) compared to the untreated tumors (grey columns). **B**) An immunopositive (Alexa564, red fluorescence) area (left) thresholded and masked (right) for defining the relative mask area (rMA = masked/annotated area). **C**) Elevated expression of TRAIL-R2 protein in the tumor cell membranes (red) both 8h and 14h post-treatment compared to the untreated tumors of the opposite legs. Please note that TRAIL-R2 expression is evenly widespread at 8h but only focal at 14h and show lower levels towards the tumor centre (asterisk) in line with the progressing tumor damage. Insets show higher power views of representative tumor areas within dashed rectangles. Cell nuclei are stained using DAPI (blue).

DOI:10.14753/SE.2015.1802

6.5.2. Stress related proteins

TMA samples from the HT29 xenograft experiment were stained using the following antibodies recognizing stress related proteins: CRT, HMGB1, Hsp70 and Hsp90.

Immunofluorescence analysis revealed elevated expression of Hsp70 between the treated and untreated group ($\chi^2(19) = 54.634$, $p < 0.05$). The post-hoc test showed significant difference between 14-24 h and 72-120 h post-treatment and a transitional decrement at 48 h. At 14h post-treatment the association of Hsp70 to the cytoplasmic membrane was significant in the treated xenografts. At later (72-120 h) stages no cytoplasmic membrane positivity was seen however, upregulation of cytoplasmic Hsp70 was observed, but only in the transient zone between the morphologically intact and dead tumor areas (**Figure 14**).

Also, significantly increased Hsp90 levels were detected ($\chi^2(21) = 83.559$, $p < 0.05$) in the mEHT treated compared to the untreated tumors, at 24, 48, 72, 120, 168 and 216 h after mEHT treatment as revealed by the post-hoc test (**Figure 15**). Hsp90 appeared in the cytoplasmic membrane only at later time points at 168 h and 216 h post-treatment. In contrast to Hsp70 kinetics, Hsp90 levels showed continuous elevation upon treatment between 24 h and 216 h.

DOI:10.14753/SE.2015.1802

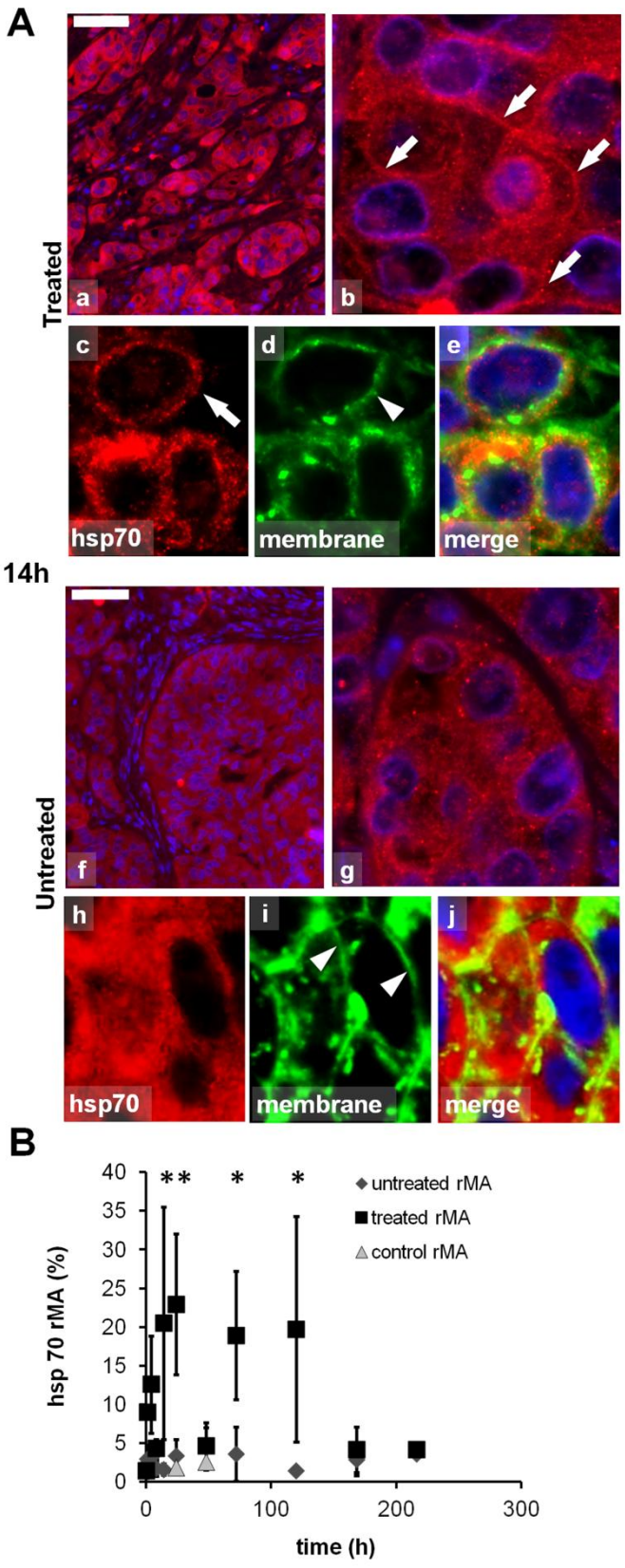

Figure 14. Abundance and localization of heat shock protein 70 (Hsp70) in colorectal cancer xenografts measured with immunofluorescence (Alexa 564, red). A) Hsp70 immunofluorescence (Alexa 564, red), in 14 h post-mEHT treated (a-e) and untreated (f-j) tumor cells also immunoreacted with wheat germ agglutinin (Alexa 488, green) and DAPI to stain nuclei. In 14 h post-mEHT treated tumor cells Hsp70 immunofluorescence is predominately in cell membranes (arrows) as indicated by the wheat germ agglutinin reactivity (arrowheads). In the untreated tumor cells Hsp70 immunofluorescence is predominately cytoplasmic. Scale bar = 80 µm in a and f, 10 µm in b and g, and 5 µm in c, d, e and h, i, j. **B)** Semi-quantitative image analysis of immunofluorescence confirms significant elevation of Hsp70 levels both between 14-24 h and 72-120 h post-treatment ($*p < 0.05$) with a decline at 48 h (rMA- relative mask area).

DOI:10.14753/SE.2015.1802

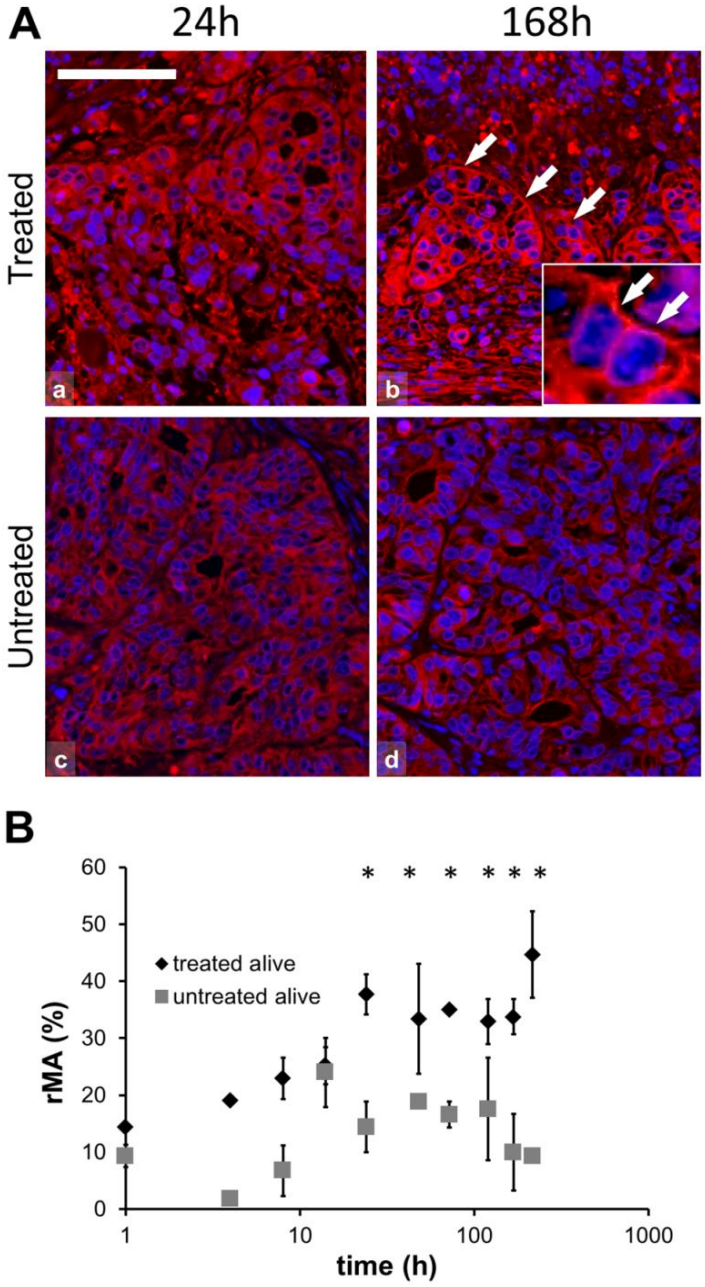

Figure 15. Heat shock protein 90 (Hsp90) immunofluorescence (Alexa 564, red) and semi-quantitative analysis of Hsp90 in post-mEHT treated and untreated colorectal cancer xenografts. A) Hsp90 immunofluorescence is predominately cytoplasmic at 24 h (a) and associated with cell membranes at 168 h post-mEHT (b; arrows), and as shown in the inset. Hsp90 immunofluorescence is less apparent at 24 h (c) and at 168 h (d) in untreated tumor cells. Cell nuclei are stained blue (DAPI). Scale bar = 60 μm in all and 20 μm in the inset. **B**) Graph showing significant increase of Hsp90 protein between 24-216 h in the treated compared to the untreated tumor cells in the morphologically intact tumor areas (*$p < 0.05$) (rMA- relative mask area).

Furthermore, the early accumulation of calreticulin to the cell membrane, before any morphological or molecular sign of programmed cell death, was observed at 4 h ($p = 0.001$) post-treatment (**Figure 16**).

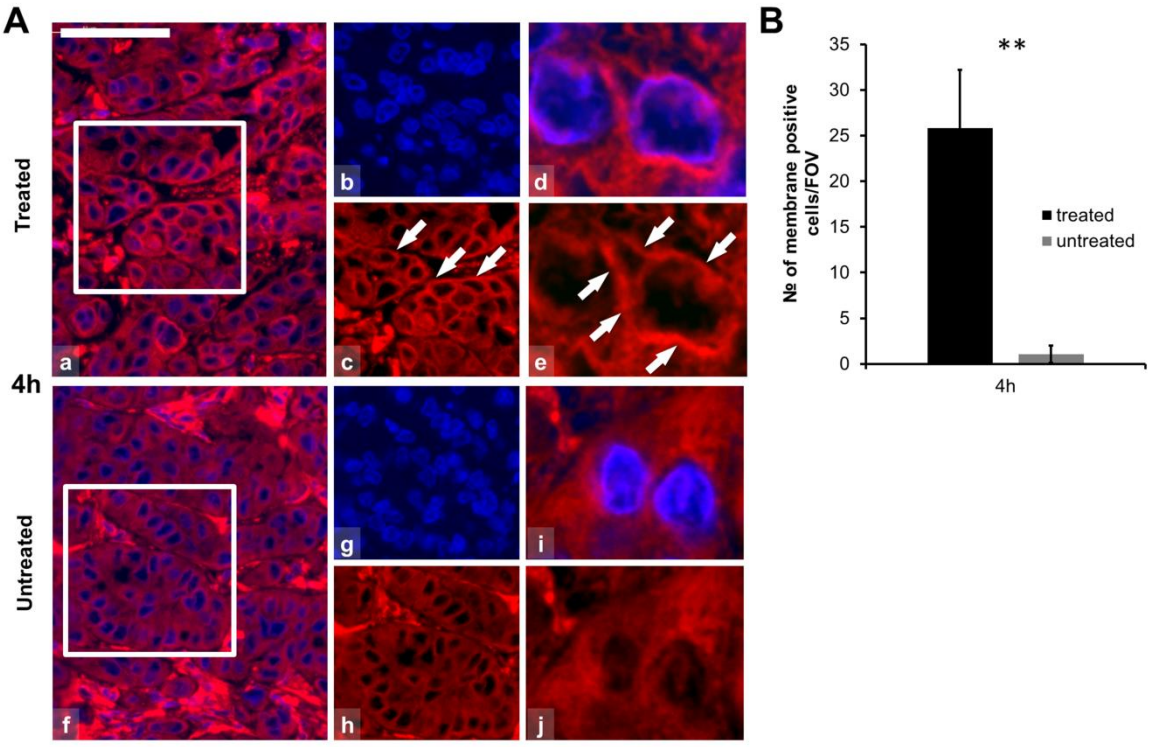

Figure 16. Calreticulin immunofluorescence (Alexa 564, red) and semi-quantitative analysis of calreticulin in post-mEHT treated and untreated colorectal cancer xenografts. A) Calreticulin immunofluorescence is localized to the cell membranes 4 h post-mEHT (arrows; a - e) before any morphological or molecular sign of programmed cell death. Calreticulin immunofluorescence is diffuse and cytoplasmic in untreated tumor cells (f - j). Cells nuclei are stained blue (DAPI). Scale bar = 60 µm in a, b, c, f, g, h and 10 µm in d, e, i, j. **B**) Graph showing the mean number of cytoplasmic membrane positive cells counted at x 100 magnification in 10 field of views (FOV) of 5 parallel samples. Elevation of calreticulin cell membrane immunofluorescence is highly significant (**$p < 0.01$) in 4 h post-mEHT treated compared to untreated tumor cells (FOV- field of views).

HMGB1 protein was detected in cell nuclei up to 14 h both in the treated and in the untreated samples, followed by a cytoplasmic translocation from 24 h in the treated xenografts. HMGB1 immunofluorescence disappeared 48 h post-treatment from the damaged central areas of the treated tumors while still prevailed in the untreated controls.

DOI:10.14753/SE.2015.1802

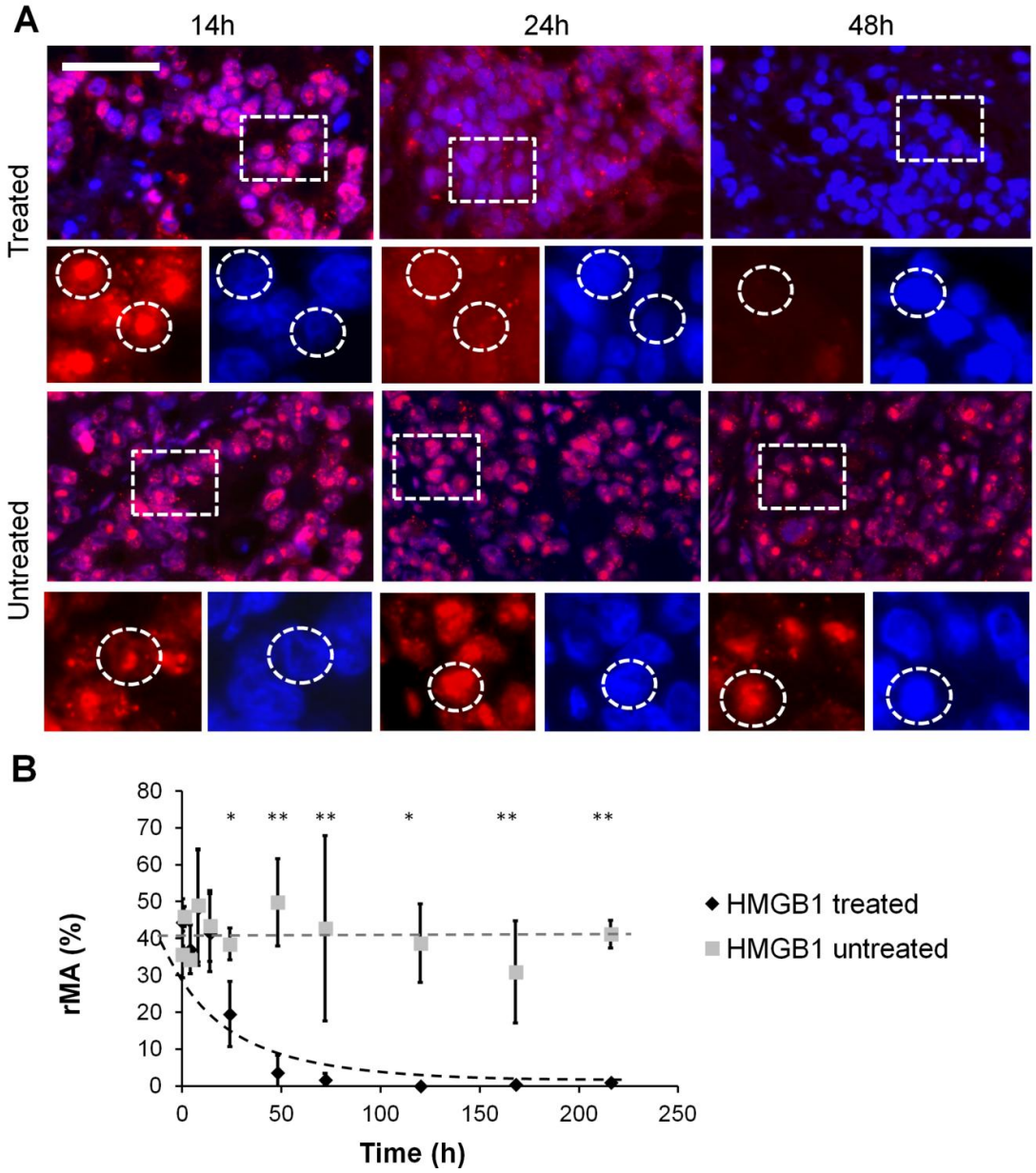

Figure 17. HMGB1 immunofluorescence (Alexa 564, red) and semi-quantitative analysis of HMGB1 post-mEHT treated and untreated colorectal cancer xenografts. A) HMGB1 immunofluorescence shows normal nuclear localization up to 14 h post-mEHT treated (a) and untreated (d) tumor cells. HMGB1 immunofluorescence is diffuse and diminished in 24 h and not evident in 48 h post-mEHT treated (b, c, respectively) tumor cells but not changed in 24 and 48 h untreated (e, f, respectively) tumor cells. Boxes show the location of the high magnification insets. Circles in the insets show the location of nuclei. Scale bar = 60 μm in a, b, c, d, e, f, and 25 μm in all insets. **B**) Semi-quantitative analysis highlights significant reduction of HMGB1 immunofluorescence between 48-216h post mEHT treated compared to untreated tumor cells (*$p < 0.05$) (rMA- relative mask area).

DOI:10.14753/SE.2015.1802

In the treated tumors nuclear HMGB1 protein was significantly lost ($\chi^2(19) = 64.657$, $p < 0.05$) compared to the untreated group, post-hoc test revealed significant difference at each time point between 24-216 h post-treatment (**Figure 17**).

6.5.3. Identification of immune cells

TMA samples from the HT29 xenograft experiment were also stained for CD3 and MPO antigens to identify major subgroups of leucocytes. The results revealed that though BALB/c (nu/nu) mice have compromised immune system featuring deficient thymic functions and T cell maturation a massive inflammatory infiltrate was observed in the treated tumors, which was concentrated at the boundary of degraded and intact tumor. The number of MPO positive neutrophil granulocytes (and monocytes) were significantly elevated in the treated samples ($\chi^2(21) = 51.364$, $p < 0.05$) compared to the controls. The post-hoc test confirmed the significant elevation at 48, 72, 120, 168 and 216 h post-treatment. The number of CD3 positive immature T lymphocytes was also significantly higher in the treated group ($\chi^2(21) = 79.949$, $p < 0.05$) than in the controls. The difference was proved significant at 120, 168 and 216 h post-treatment (**Figure 18**).

DOI:10.14753/SE.2015.1802

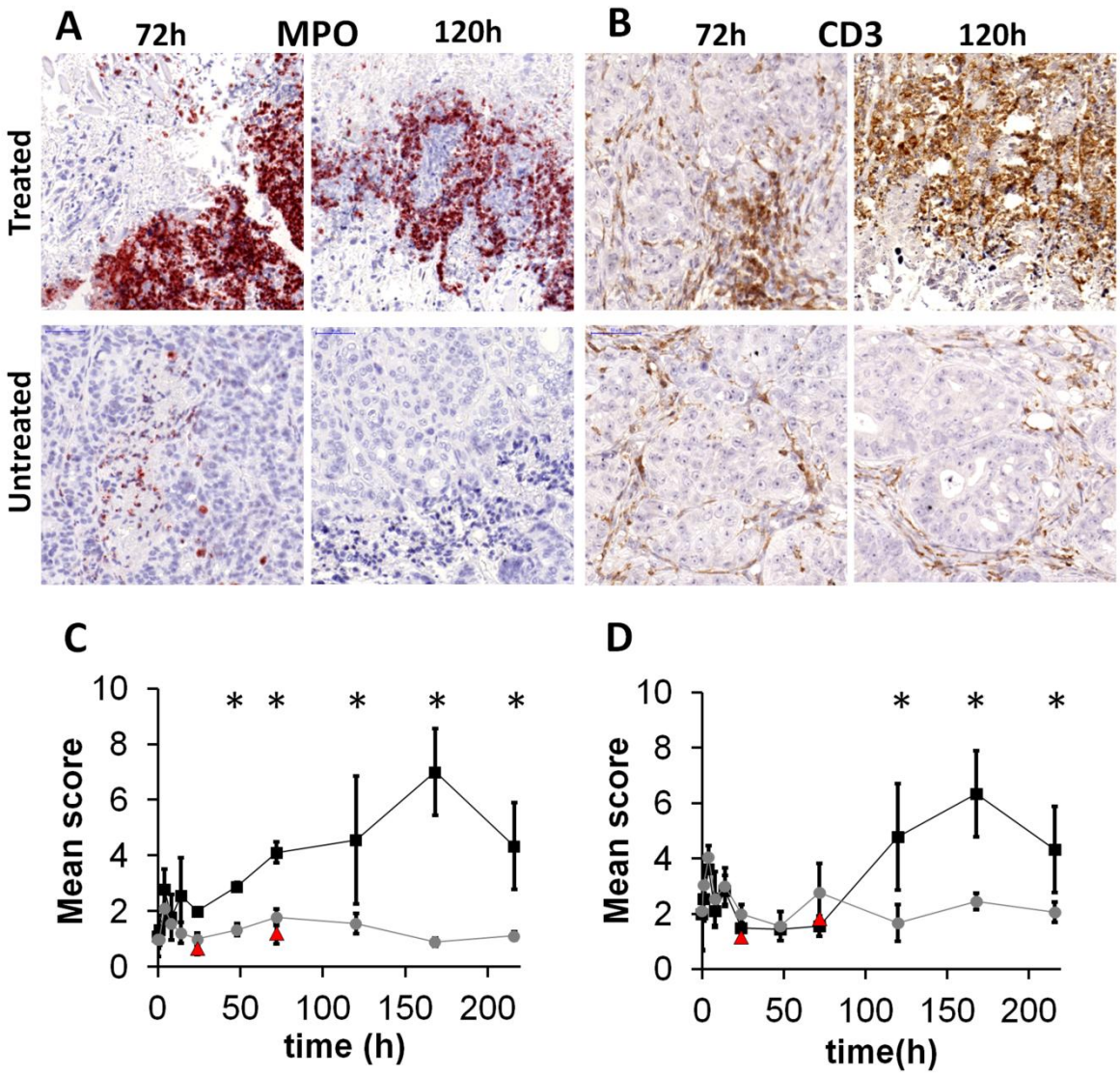

Figure 18. Leukocyte infiltration detected with immunohistochemistry upon mEHT treatment of HT29 colorectal cancer xenografts. **A-B**) The number of both the myeloperoxidase (MPO - red) positive neutrophil granulocytes (**A**) and the CD3 positive (brown) T lymphocytes (**B**) are significantly elevated in the treated compared to the untreated tumors at 72 h (only for MPO) and 120 h (both markers) post-treatment. **C-D**) Graphs show the dynamic treatment related appearance of MPO positive cells (**C**) and CD3 positive cells **(D**) during the study period. Peritumoral infiltration by myeloid leukocytes (**C**) start very early (after 1h), while T cell accumulation is observed after 72 h and both show significant treatment related elevation afterwards. Black boxes represent the mean scores in the treated tumors and grey boxes highlight scores gained in the untreated controls. Red triangles show leukocyte scores in xenografts of sham-treated animals.

DOI:10.14753/SE.2015.1802

7. DISCUSSION

Electric field and the concomitant heat induced by modulated electrohyperthermia (mEHT) can be selectively enriched in malignant tissue due to elevated glycolysis (Warburg effect), ion concentration and the resulting elevated conductivity and permittivity in cancer compared to non-malignant tissues. The objective of this study was to investigate the nature and time course of tumor cell destruction, its molecular mechanism and the stress-related molecular changes induced by mEHT in HT29 colorectal cancer xenograft model.

Modulated EHT is a non-invasive technique in oncotherapy using 13.56 MHz capacitive coupled radiofrequency field. The generated electric field selectively enriches in the malignant tumor tissue due to the bioelectrodynamic differences (such as elevated permittivity and conductivity) related to metabolic (Warburg-effect and the concomitant elevation in ion concentration) and structural differences (such as increased water and sodium content and altered membrane permeability) compared to non-malignant tissue (Pethig et al. 1984; Scholoz et al. 2000; Andocs et al. 2009). Our results in this project are based on morphological observations, mRNA expression microarray studies, *in vitro* (protein array chip and Western immunoblot) and *in situ* (immunoperoxidase and immunofluorescence) protein detection studies combined with digital microscopy based semiquantitative image analysis and the TUNEL assay.

Comparative analysis of hematoxylin and eosin stained sections across the center of tumor xenografts revealed significant tumor destruction between 24-120 h after a 30 min long single shot of mEHT treatment. At this stage, we did not discriminate between the different types of cell death subroutines (apoptosis, necroptosis, accidental necrosis, autophagia, etc). The peak of tumor destruction reached a 7-fold increase at 72 h post-treatment compared to the untreated contralateral xenograft. Significant appearance of apoptotic bodies were observed 48-72 h post-treatment, and TUNEL positivity, referring to DNA fragmentation, was found the highest at 24-48 h post-treatment. Chromatin condensation, the appearance of discrete nuclear bodies and the signs of the DNA fragmentation together suggested programmed cell death (Kroemer et al. 2009) as the major mechanism of tumor destruction upon mEHT treatment. Hyperthermia was described to be suitable to induce both accidental

necrosis and programmed cell death *in vitro* in a temperature dependent manner without specifying the dose related response (Hildebrandt et al. 2002). Most of the apoptotic cell death inducing treatments were achieved in hematological cell lines (Harmon et al. 1990; Baxter et al. 1992; Gabai et al. 1995) which are known to be rather thermo-sensitive (Hildebrandt et al. 2002). In these studies the molecular mechanism of cell death was not described in details, and the results were rather contradictory. As opposed to our findings, *in vitro* hyperthermia delivered in a 42 °C incubator or in a water bath, could not induce DNA fragmentation in HT29 colorectal carcinoma cells up to 72 h post-treatment (Nishida et al. 1997; Shchepotin et al. 1997).

Because both the morphological and molecular signs suggested DNA fragmentation and programmed cell death mechanisms we have tested molecules that might be involved and characteristic of the major programmed cell death pathways. The mitochondrial accumulation of pro-apoptotic Bcl-2 superfamily member Bax was found to be significant between 8-14 h post-treatment in the treated tumors compared to the contralateral untreated xenografts. In line with the morphological findings, mitochondrial Bax was consistent with a controlled outer mitochondrial membrane pore formation, which further supported the programmed nature of the treatment induced cell death (Gogvadze et al. 2006; Basanez et al. 2012; Galluzzi et al. 2012). Due to the mitochondrial pores intermembrane space proteins can also be released from the mitochondria (Tait et al. 2010). Accordingly, significant mitochondrial to cytoplasmic cytochrome c release was observed between 8-14 h post-treatment, simultaneously with mitochondrial Bax accumulation, reflecting the rapid cytoplasmic release of cytochrome c (Basanez et al. 2012). At 8 h post-treatment elevated expression of the intermembrane space proteins Smac/Diablo and HTRA2/Omi were also detected, as a further support of the cytoplasmic release of intermembrane space proteins (Tait et al. 2010). Mitochondrial pore formation, and concomitant loss of mitochondrial transmembrane potential, together with the release of intermembrane space proteins to the cytoplasm can lead to an irreversible “point of no return” in the fate of affected cells (Kroemer et al. 2005; Kroemer et al. 2009). Between 14-24 h post-treatment mitochondrial AIF was released to the nucleus, where the 57 kDa activated AIF fragment was also detected using immunoblots. AIF release from the mitochondria requires a

cleavage in the mitochondrial intermembrane space (Norberg et al. 2010), and a concomitant time delay can be noted compared to the pore formation and mitochondrial protein release (Norberg et al. 2010). Activated nuclear AIF fragments are responsible for chromatin condensation and cleavage of the DNA into relatively large 50 kbp fragments (Boujrad et al. 2007), which were detected with the TUNEL assay at later time points.

Modulated EHT induced programmed cell death in HT29 xenograft in a caspase independent manner, since cleaved caspase-3 protein was not found in the tumor cells at any tested time point. Although detected cleaved-caspase 3 levels were significantly higher in the treated whole tumor samples compared to the untreated control xenografts, immunohistochemistry revealed that cleaved caspase-3 positive cells were found only in stromal inflammatory cells adjacent to tumor nests. These cells were consistently MPO positive myelomonocytic cells primarily of neutrophil granulocytes and CD3 immature T lymphocytes (immunocompromised animals). Leukocytes are known to be sensitive for heat shock (Hildebrandt et al. 2002; Dieing et al. 2003), which can explain their relatively high cleaved caspase-3 positivity. The timing and major molecular pathways involved in mEHT treatment related tumor cell death are summarized in a simplified scheme in **Figure 19**.

When markers for necroptosis (programmed necrosis) were analyzed, no significant difference was found at any time point either in RIP1 or RIP3 expression between treated and untreated tumors. RIP1 and RIP3 are crucial members of the necrosome complex (Vandenabeele et al. 2010), which can be activated by phosphorylation. RIP1 at Ser161 can be either autophosphorylated or phosphorylated by RIP3, which can also be phosphorylated on Ser199 for activation (Vandenabeele et al. 2010; Han et al. 2011). Although RIP3 seems to be necessary for regulated necrosis it can be either dependent or independent on RIP1 (Vandenabeele et al. 2010; Han et al. 2011; Galluzzi et al. 2012). RIP1 and RIP3 can be inactivated by proteolytic cleavage resulting in the shifting of cell degradation pathway to external apoptosis. Despite the extensive research the exact downstream mechanism of regulated necrosis has not been clarified yet (Christofferson et al. 2010; Han et al. 2011).

The lack of massive cytoplasmic vacuolization and the proven Bax mediated mitochondrial pore formation rule out the possibility of autophagic cell death (Galluzzi et al. 2012).

DOI:10.14753/SE.2015.1802

Interestingly, preliminary results of mEHT treated C26 (murine colorectal carcinoma cell line) allografts suggest rather a caspase dependent cell death pathway. Therefore, further investigations are needed for revealing the factors that determine the different programmed cell death subroutines.

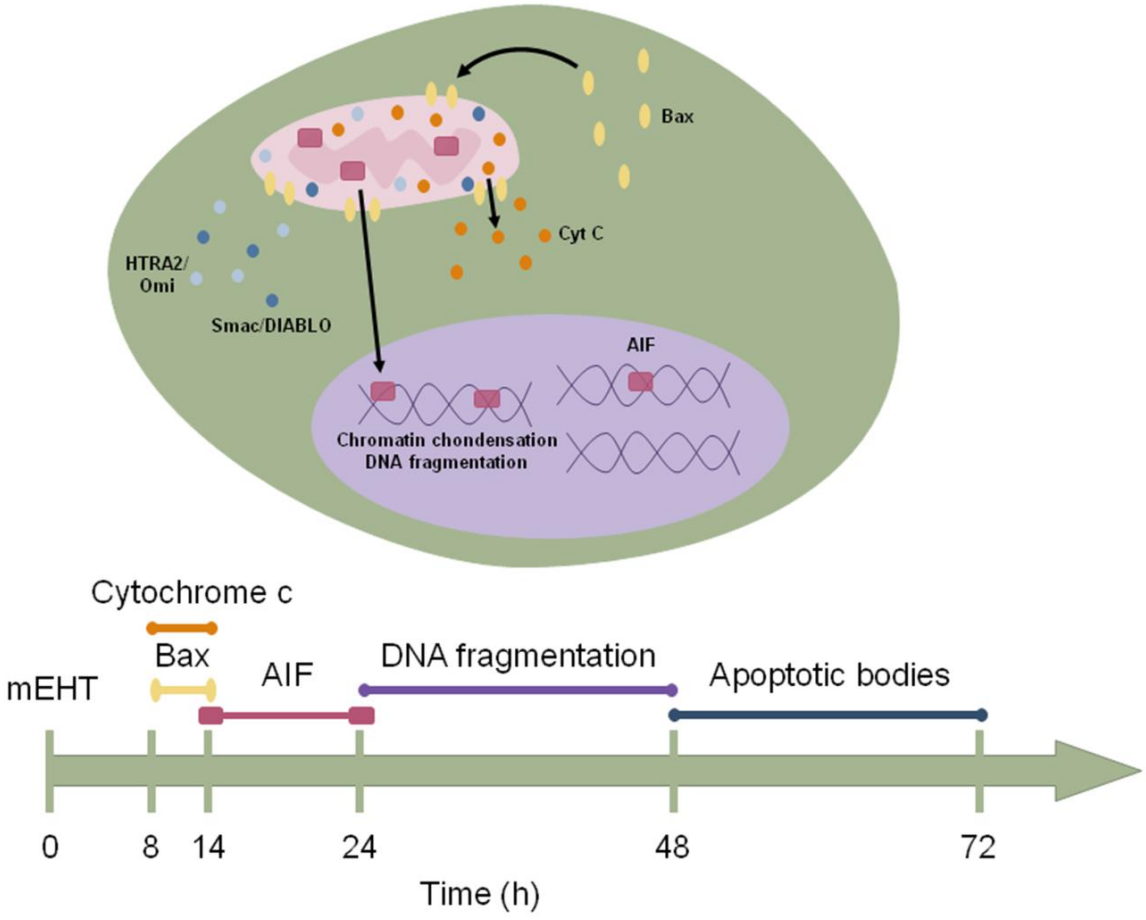

Figure 19. Schema of mEHT induced programmed cell death mechanism in HT29 xenograft model. Treatment related mitochondrial pore formation was observed 8-14 h post-treatment by Bax mitochondrial localization, in line with this cytochrome c released from the mitochondria. Concomitant nuclear AIF induced DNA fragmentation followed by apoptotic body formation.

As it was described earlier ICD requires a characteristic spatiotemporal emergence of a DAMP signal sequence including the early (pre-apoptotic) exposure of calreticulin to the cell surface as ecto-calreticulin, followed by a membrane localization and release of Hsp70 and/or Hsp90 accompanied by ATP release during the programmed cell death process, the

late apoptotic release of HMGB1 and possible late externalization of Hsp70 and or Hsp90 (Garg et al. 2013; Kroemer et al. 2013; Krysko et al. 2013). Different ICD inducers can provoke slightly distinct DAMP patterns. For example, oxaliplatin can initiate the pre-apoptotic ecto-calreticulin exposure, followed by an early-apoptotic ATP release without Hsp involvement, with late apoptotic HMGB1 release (Ladoire et al. 2013). Another example is hypericin based photodynamic therapy, which induces pre-apoptotic ecto-calreticulin exposure and ATP release with pre-apoptotic Hsp70 membrane appearance and the passive, late-apoptotic release of Hsp70, Hsp90 and HMGB1 (Garg et al. 2012; Krysko et al. 2012).

In our HT29 colorectal xenograft model a significant early (4 h post-treatment) cell membrane exposure of calreticulin was detected in the treated compared to the contra-lateral untreated tumors. The first molecular signs of programmed cell death were revealed later at 8 h post-treatment. Ecto-calreticulin can serve as an ‘eat-me’ signal which can bind to DCs and macrophages through CD91 to stimulate the efficient engulfing of dying cells, and processing their antigens followed by priming a connate immune response (Kroemer et al. 2013).

Hsp70 was found in the cytoplasmic membranes of tumor cells from 14 h post-treatment followed by a decrement at 48 h with a second peak observed at 72 h post-treatment in the morphologically intact peripheral part of mEHT treated xenografts. This second peek is possibly related to the soluble factors released from the mEHT damaged cells. Significant elevation of Hsp90 was observed from 24h post-treatment but membrane association of Hsp90 was observed only at later time points (168-216 h). Interactions of membrane associated Hsp70 with immune cells can be rather complex. Membrane associated Hsp70 combined with IL-2 and IL-15 can stimulate natural killer (NK) cells (Gehrmann et al. 2008). Membrane bound Hsp70-peptide complex possibly bind to scavenger receptors, C-type lectin receptor or TLR 2/4 or a currently not well defined receptor on APCs including monocytes, macrophages and DC followed by cross presentation on MHC molecules to initiate antigen specific immune response through CD8+ T cells (Multhoff 2007; Gehrmann et al. 2008). Extracellular Hsp70 can directly boost the innate immune response (Multhoff et al. 2011). However, membrane bound Hsp70 has also been described

to protect cell membrane integrity under stress condition (Horvath et al. 2008; Horvath et al. 2010), therefore, the outcome of cell membrane exposure of Hsp70 can be context dependent. Membrane associated Hsp90 binding receptors on APCs have not been identified yet (Garg et al. 2013).

The late HMGB1 release from cell nuclei was observed from 24 h post-treatment showing first a cytoplasmic manifestation in the mEHT destructed central tumor areas. HMGB1 staining was worn off between 48-216 h post-treatment. Given that HMGB1 can also be released passively from the necrotic cells nuclei (Guo et al. 2013), necrotic areas of untreated tumors also showed moderate HMGB1 disappearance. The mEHT related spatiotemporal appearance of DAMP signals, which can be relevant to ICD in the HT29 xenograft model is summarized in a drawing (**Figure 20**).

Earlier, HMGB1 was thought to be released only from the necrotic cells, recent evidence suggest that cells dying through a programmed cell death subroutine can also release HMGB1 (Ladoire et al. 2013). The extracellular HMGB1 can bind to RAGE, TIM3 or TLR2/4 on the DCs leading to distinct responses (Garg et al. 2013). HMGB1-RAGE interaction may mediate invasion, migration and tumor growth resulting in the association with aggressive tumor phenotype and poor prognosis in colon carcinoma (Ladoire et al. 2013). HMGB1 binding to TIM3 can also suppress the immunostimulatory pathway in DCs. HMGB1-TLR2/4 interaction is essential for determining the immunogenicity of the dying tumor through cross presentation of the tumor antigens and promotion of the tumor specific Tc1/Th1 cell responses (Ladoire et al. 2013).

We have found CD3 positive T lymphocytes (between 120-216 h post-treatment) and MPO positive neutrophil granulocytes/monocytes (between 72-216 h post-treatment) demarcating the destructed central tumor areas in mEHT treated xenografts. These inflammatory infiltrates can be consistent with the immunostimulatory effects of HMGB1 release from the nucleus and beyond (Ladoire et al. 2013).

As it has become clear the ultimate outcome of DAMP related immune response to cancer cell death is rather complex and context dependent. Cell death is influenced by the type and localization/microenvironment of cancer cells, the cell death pathways activated, the type of immune cells interacting with the cancer and the efficiency of the recognition of cancer

antigens (Garg et al. 2013). In this project we used immunodeficient Balb/c (nu/nu) mice lacking mature T cells to host HT29 colorectal cancer xenografts. Therefore, this model is inappropriate for investigating proper immune response upon mEHT treatment thus the detected DAMP signals cannot be linked directly to ICD. However, the DAMP signal sequence revealed in this model support the feasibility of testing if mEHT treatment in immune competent animal models can directly promote ICD.

Furthermore, some of the chemotherapeutic ICD inducers are already used on daily bases, but in combination with corticosteroids, which may demolish the potential immune response (Kepp et al. 2011). If a local treatment can induce DAMP and consequently ICD these may give rise to effective anti-tumor immune response. On the other hand mEHT treatment might destroy locally the leucocytes as suggested by elevated expression of caspase-3 in these cells, but does not eradicate them on a systemic level.

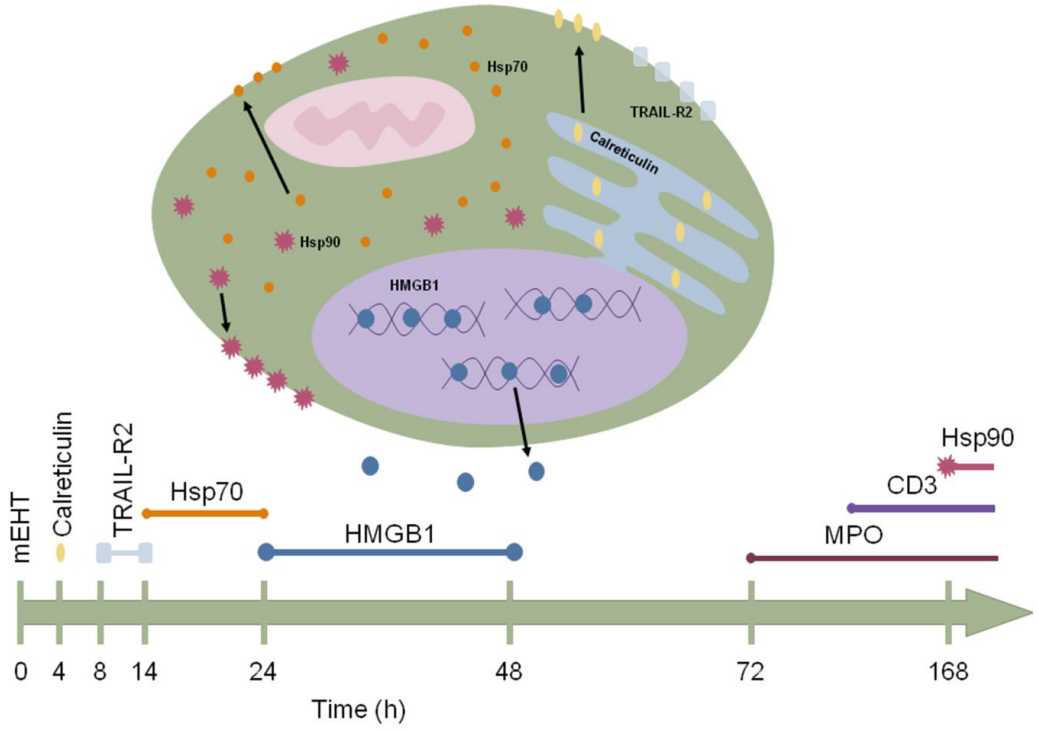

Figure 20. Schema of mEHT induced spatiotemporal appearance of DAMP related to ICD in HT29 xenograft model. Modulated EHT induced ecto-calreticulin exposure, Hsp70 membrane appearance, followed by nuclear HMGB1 release and Hsp90 membrane translocation. Concomitant MPO and CD3 positive leukocyte were detected around the destructed tumor area.

Finally, as an important observation we found the significant elevation of TRAIL-R2 a pro-apoptotic receptor mediating extrinsic programmed cell death signal, between 8-14 h post-treatment. This can either be a direct consequence of the treatment, then the cell death subroutine should be external apoptosis mediated by caspase-8 or necroptosis mediated by RIP1 or RIP3 (Jouan-Lanhouet et al. 2012). TRAIL-R2 externalization can be a secondary effect related to the ER stress induced by unfolded protein response (Stolfi et al. 2012). The lack of caspase-8 cleavage or RIP1 or RIP3 activation leads to the conclusion that TRAIL-R2 elevation is more probably a secondary event (Jouan-Lanhouet et al. 2012). Heat may induce endoplasmic reticulum stress related unfolded protein response (Adachi et al. 2009), which can induce elevated TRAIL-R2 expression even in p53 mutant cell lines such as colorectal cancer cell lines including HT29 (Stolfi et al. 2012). This is further supported by that TRAIL-R2 positivity was observed in the periphery of the tumor 14 h post-treatment where no mitochondrial Bax or cytoplasmic cytochrome c release was observed. In line with this, a decrement in survivin was measured on the apoptosis protein arrays as it has also been referred in the literature (Stolfi et al. 2012). TRAIL upregulation upon mEHT treatment can potentially be exploited for potentiating TRAIL-R2 agonist tumor treatment with mEHT (Hellwig et al. 2012). Obviously, further investigations are required for revealing the endoplasmic reticulum stress related unfolded protein response. Furthermore, for an adequate therapeutic response through TRAIL or TRAIL agonists testing the pattern of decoy receptors (DcR1 and DcR2) is also crucial. TRAIL is the ligand of decoy receptors, however, decoy receptors lack death domains, therefore, the downstream signaling for any programmed cell death subroutine is insufficient through them. Not surprisingly, DcR1 and DcR2 can inhibit TRAIL-R1 and TRAIL-R2 (Wang 2010).

In summary, mEHT treatment can induce programmed cell death related tumor destruction in HT29 colorectal adenocarcinoma xenografts, which dominantly follows a caspase independent subroutine in line with spatiotemporal DAMP sequence that may be relevant for promoting immunological cell death.

DOI:10.14753/SE.2015.1802

8. CONCLUSION – NEW OBSERVATIONS

1. A single shot mEHT treatment in an *in vivo* HT29 xenograft raised in Balb/c (nu/nu) mice cause significant tumor cell destruction with a peak of 7-fold increase at 72 h post-treatment compared to the untreated control tumors.

2. Programmed cell death induced by mEHT in HT29 xenograft dominantly follows a caspase independent subroutine with mitochondrial permeabilization by Bax, the cytoplasmic release of cytochrome c and concomitant mitochondrial to nuclear translocation and activation of AIF resulting in DNA fragmentation as measured with the TUNEL assay.

3. A single shot mEHT treatment related tumor cell stress can generate the spatiotemporal sequence of DAMP signals in the HT29 colorectal cancer xenograft model without any additional genetic or pharmaceutical intervention. Our data suggest that mEHT can be a potential local inducer of ICD, without a systemic interference with immune functions.

DOI:10.14753/SE.2015.1802

9. SUMMARY

Electric field and concomitant heat induced by modulated electrohyperthermia (mEHT) can be selectively enriched in malignant tissue due to elevated glucolysis (Warburg effect), resulting in elevated conductivity and permittivity in cancer compared to non-malignant tissue. In this project we studied the mechanism and time course of tumor destruction and focused on spatiotemporal appearance of damage associated molecular pattern (DAMP) related to mEHT.

Bilateral implants of HT29 colorectal cancer in the femoral regions of Balb/c (nu/nu) mice were treated with a single 30 min shot of mEHT. Tumors at 0, 1, 4, 8, 14, 24, 48, 72, 120, 168 and 216 h post-treatment were studied for morphology, DNA fragmentation and cell death response related protein expression using tissue microarrays, immunohistochemistry, western immunoblots and mRNA microarrays.

Modulated EHT treatment induced significant tumor destruction in HT29 xenografts with a peak of 7-fold increase compared to the untreated controls. The significant treatment related elevation of DNA fragmentation and apoptotic bodies between 24-72 h post-treatment proved a programmed cell death response. This was associated with significant mitochondrial accumulation of Bax and cytoplasmic release of cytochrome c proteins between 8-14 h. Cleaved caspase-3 levels were low and mainly localized to inflammatory cells. The substantial cytoplasmic to nuclear translocation of 57 kDa activated fragment of apoptosis inducing factor was detected between 14-24 h. The cell death response was accompanied by the 4 h post-treatment upregulation of heat shock protein mRNA levels. The treatment resulted in spatiotemporal occurrence of a DAMP featured by significant cytoplasmic to cell membrane translocation of calreticulin at 4 h, Hsp70 between 14-24 h and Hsp90 at 216 h post-treatment. The release of high mobility group box1 protein from tumor cell nuclei from 24 h post-treatment was also detected.

Modulated EHT treatment can induce programmed cell death related tumor destruction in HT29 colorectal adenocarcinoma xenografts, which dominantly follows a caspase independent subroutine in line with spatiotemporal DAMP sequence that may be relevant for promoting immunological cell death.

DOI:10.14753/SE.2015.1802

10. ÖSSZEFOGLALÁS

Az elektromos tér és az általa generált hő (modulált elektrohipertermia- mEHT) szelektíven dúsul a malignus szövetben. A daganatos szövet megváltozott metabolizmusa, aerob glikolízis (Warburg hatás) hatására a malignus szövet vezetőképessége és permittivitása emelkedett a malignusan nem elfajult szövethez képest. Jelen tanulmányban a mEHT sejtpusztító hatás molekuláris szintű hatásmechanizmusát, valamint az immunogén sejthalálra (ICD) jellemző molekuláris mintázatot (DAMP) vizsgáltuk.

A kísérletekhez HT29 kolorektális adenocarcinoma sejtvonalat injektáltunk Balb/c (nu/nu) egerek mindkét oldali femorális régiójába. A jobb oldali tumorokat egyszeri 30 perces, mEHT-val kezeltünk. A mintavételezés 0, 1, 4, 8, 14, 24, 48, 72, 120, 168 és 216 órával a kezelést követően történt. A minták morfológiai, mRNS expressziós, DNS fragmentációs vizsgálatára, valamint a sejthalállal kapcsolatos fehérjék expressziójának analízisére került sor western blottal valamint szöveti multiblokkokon immunperoxidáz és immunfluoreszcencia vizsgálatokkal.

A morfológiai vizsgálatok alapján megállapítottuk, hogy a mEHT kezelés HT29 xenograftokban maximálisan hétszeres sejtelhalást eredményezett a kezeletlen tumorokhoz képest. A kezelés hatására szignifikáns DNS fragmentációt és apoptotikus testek megjelenését detektáltuk 24–72 órával a kezelést követően. 8–14 órával a kezelés után a pro-apoptotikus Bax mitokondriális felhalmozódását és a citokróm-c mitokondriumból való kiáramlását észleltük. Ugyanakkor hasított kaszpáz-3 pozitív sejteket kizárólag a MPO vagy CD3 pozitív gyulladásos sejtekben találtunk. 14–24 órával a kezelést követően az apoptózis indukáló factor 57 kDa-os fragmentjét detektáltuk western blottal és sejtmagi előfordulását imunnhisztokémiai vizsgálattal. 4 órával a kezelést követően hő sokk fehérjék mRNS szintű szignifikáns emelkedését detektáltuk. Fehérje szinten DAMP mintázatot is észleltünk, így citoplazma membrán dúsulását detektáltunk 4 órával a kezelést követően a karetikulin, 14-24 óránál a Hsp70 és 216 óránál a Hsp90 esetében. A sejtmagokból a HMGB1 kiáramlás 24 órával a kezelést követően kezdődött.

Összefoglalva: a HT29 humán kolorektális adenokarcinóma modellben a mEHT kezelés elsősorban kaszpáz független programozott sejthalált váltott ki és egyidejűleg indukálta az immunogén sejthalálra jellemző DAMP megjelenését.

11. BIBLIOGRAPHY

Adachi, M., Liu, Y., Fujii, K., Calderwood, S. K., Nakai, A., Imai, K. and Shinomura, Y. (2009). "Oxidative stress impairs the heat stress response and delays unfolded protein recovery." PLoS One **4**(11): e7719.

Adachi, S., Kokura, S., Okayama, T., Ishikawa, T., Takagi, T., Handa, O., Naito, Y. and Yoshikawa, T. (2009). "Effect of hyperthermia combined with gemcitabine on apoptotic cell death in cultured human pancreatic cancer cell lines." Int J Hyperthermia **25**(3): 210-219.

Andocs, G., Renner, H., Balogh, L., Fonyad, L., Jakab, C. and Szasz, A. (2009). "Strong synergy of heat and modulated electromagnetic field in tumor cell killing." Strahlenther Onkol **185**(2): 120-126.

Aoyagi, T., Terracina, K. P., Raza, A. and Takabe, K. (2014). "Current treatment options for colon cancer peritoneal carcinomatosis." World J Gastroenterol **20**(35): 12493-12500.

Atmaca, A., Al-Batran, S. E., Neumann, A., Kolassa, Y., Jager, D., Knuth, A. and Jager, E. (2009). "Whole-body hyperthermia (WBH) in combination with carboplatin in patients with recurrent ovarian cancer - a phase II study." Gynecol Oncol **112**(2): 384-388.

Barsukov, Y. A., Gordeyev, S. S., Tkachev, S. I., Fedyanin, M. Y. and Perevoshikov, A. G. (2013). "Phase II study of concomitant chemoradiotherapy with local hyperthermia and metronidazole for locally advanced fixed rectal cancer." Colorectal Dis **15**(9): 1107-1114.

Basanez, G., Soane, L. and Hardwick, J. M. (2012). "A new view of the lethal apoptotic pore." PLoS Biol **10**(9): e1001399.

Baxter, G. D. and Lavin, M. F. (1992). "Specific protein dephosphorylation in apoptosis induced by ionizing radiation and heat shock in human lymphoid tumor lines." J Immunol **148**(6): 1949-1954.

Blad, B. and Baldetorp, B. (1996). "Impedance spectra of tumour tissue in comparison with normal tissue; a possible clinical application for electrical impedance tomography." Physiol Meas **17 Suppl 4A**: A105-115.

Blank, M. and Goodman, R. (2009). "Electromagnetic fields stress living cells." Pathophysiology **16**(2-3): 71-78.

Boujrad, H., Gubkina, O., Robert, N., Krantic, S. and Susin, S. A. (2007). "AIF-mediated programmed necrosis: a highly regulated way to die." Cell Cycle **6**(21): 2612-2619.

Brazma, A., Hingamp, P., Quackenbush, J., Sherlock, G., Spellman, P., Stoeckert, C., Aach, J., Ansorge, W., Ball, C. A., Causton, H. C., Gaasterland, T., Glenisson, P., Holstege, F. C., Kim, I. F., Markowitz, V., Matese, J. C., Parkinson, H., Robinson, A., Sarkans, U., Schulze-Kremer, S., Stewart, J., Taylor, R., Vilo, J. and Vingron, M. (2001). "Minimum information about a microarray experiment (MIAME)-toward standards for microarray data." Nat Genet **29**(4): 365-371.

Calderwood, S. K. (2013). "Molecular cochaperones: tumor growth and cancer treatment." Scientifica (Cairo) **2013**: 217513.

Castano, A. P., Mroz, P. and Hamblin, M. R. (2006). "Photodynamic therapy and anti-tumour immunity." Nat Rev Cancer **6**(7): 535-545.

Chen, F., Wang, C. C., Kim, E. and Harrison, L. E. (2008). "Hyperthermia in combination with oxidative stress induces autophagic cell death in HT-29 colon cancer cells." Cell Biol Int **32**(7): 715-723.

Cheung, A. Y. (1982). "Microwave and radiofrequency techniques for clinical hyperthermia." Br J Cancer Suppl **5**: 16-24.

Chicheł, A., Skowronek, J., Kubaszewska, M. and Kanikowski, M. (2007). "Hyperthermia – description of a method and a review of clinical applications." Reports of Practical Oncology & Radiotherapy **12**(5): 267-275.

Christofferson, D. E. and Yuan, J. (2010). "Necroptosis as an alternative form of programmed cell death." Curr Opin Cell Biol **22**(2): 263-268.

Chua, T. C., Robertson, G., Liauw, W., Farrell, R., Yan, T. D. and Morris, D. L. (2009). "Intraoperative hyperthermic intraperitoneal chemotherapy after cytoreductive

surgery in ovarian cancer peritoneal carcinomatosis: systematic review of current results." J Cancer Res Clin Oncol **135**(12): 1637-1645.

Csoboz, B., Balogh, G. E., Kusz, E., Gombos, I., Peter, M., Crul, T., Gungor, B., Haracska, L., Bogdanovics, G., Torok, Z., Horvath, I. and Vigh, L. (2013). "Membrane fluidity matters: hyperthermia from the aspects of lipids and membranes." Int J Hyperthermia **29**(5): 491-499.

D'Eliseo, D., Manzi, L. and Velotti, F. (2013). "Capsaicin as an inducer of damage-associated molecular patterns (DAMPs) of immunogenic cell death (ICD) in human bladder cancer cells." Cell Stress Chaperones.

Denecker, G., Vercammen, D., Declercq, W. and Vandenabeele, P. (2001). "Apoptotic and necrotic cell death induced by death domain receptors." Cell Mol Life Sci **58**(3): 356-370.

Dewey, W. C. (1994). "Arrhenius relationships from the molecule and cell to the clinic." Int J Hyperthermia **10**(4): 457-483.

Dewey, W. C., Hopwood, L. E., Sapareto, S. A. and Gerweck, L. E. (1977). "Cellular responses to combinations of hyperthermia and radiation." Radiology **123**(2): 463-474.

Dieing, A., Ahlers, O., Kerner, T., Wust, P., Felix, R., Loffel, J., Riess, H. and Hildebrandt, B. (2003). "Whole body hyperthermia induces apoptosis in subpopulations of blood lymphocytes." Immunobiology **207**(4): 265-273.

Elmore, S. (2007). "Apoptosis: a review of programmed cell death." Toxicol Pathol **35**(4): 495-516.

Feyerabend, T., Wiedemann, G. J., Jager, B., Vesely, H., Mahlmann, B. and Richter, E. (2001). "Local hyperthermia, radiation, and chemotherapy in recurrent breast cancer is feasible and effective except for inflammatory disease." Int J Radiat Oncol Biol Phys **49**(5): 1317-1325.

Fiorentini, G., Giovanis, P., Rossi, S., Dentico, P., Paola, R., Turrisi, G. and Bernardeschi, P. (2006). "A phase II clinical study on relapsed malignant gliomas treated with electro-hyperthermia." In Vivo **20**(6A): 721-724.

Fiorentini, G. and Szasz, A. (2006). "Hyperthermia today: electric energy, a new opportunity in cancer treatment." J Cancer Res Ther **2**(2): 41-46.

Foster, K. R. (2000). The biomedical Engineering Handbook: SecondEdition, CRC Press.

Gabai, V. L., Zamulaeva, I. V., Mosin, A. F., Makarova, Y. M., Mosina, V. A., Budagova, K. R., Malutina, Y. V. and Kabakov, A. E. (1995). "Resistance of Ehrlich tumor cells to apoptosis can be due to accumulation of heat shock proteins." FEBS Lett **375**(1-2): 21-26.

Galluzzi, L., Vitale, I., Abrams, J. M., Alnemri, E. S., Baehrecke, E. H., Blagosklonny, M. V., Dawson, T. M., Dawson, V. L., El-Deiry, W. S., Fulda, S., Gottlieb, E., Green, D. R., Hengartner, M. O., Kepp, O., Knight, R. A., Kumar, S., Lipton, S. A., Lu, X., Madeo, F., Malorni, W., Mehlen, P., Nunez, G., Peter, M. E., Piacentini, M., Rubinsztein, D. C., Shi, Y., Simon, H. U., Vandenabeele, P., White, E., Yuan, J., Zhivotovsky, B., Melino, G. and Kroemer, G. (2012). "Molecular definitions of cell death subroutines: recommendations of the Nomenclature Committee on Cell Death 2012." Cell Death Differ **19**(1): 107-120.

Garg, A. D., Krysko, D. V., Vandenabeele, P. and Agostinis, P. (2012). "Hypericin-based photodynamic therapy induces surface exposure of damage-associated molecular patterns like HSP70 and calreticulin." Cancer Immunol Immunother **61**(2): 215-221.

Garg, A. D., Martin, S., Golab, J. and Agostinis, P. (2013). "Danger signalling during cancer cell death: origins, plasticity and regulation." Cell Death Differ.

Garg, A. D., Nowis, D., Golab, J., Vandenabeele, P., Krysko, D. V. and Agostinis, P. (2010). "Immunogenic cell death, DAMPs and anticancer therapeutics: an emerging amalgamation." Biochim Biophys Acta **1805**(1): 53-71.

Gehrmann, M., Radons, J., Molls, M. and Multhoff, G. (2008). "The therapeutic implications of clinically applied modifiers of heat shock protein 70 (Hsp70) expression by tumor cells." Cell Stress Chaperones **13**(1): 1-10.

Genet, S. C., Fujii, Y., Maeda, J., Kaneko, M., Genet, M. D., Miyagawa, K. and Kato, T. A. (2013). "Hyperthermia inhibits homologous recombination repair and sensitizes cells to ionizing radiation in a time- and temperature-dependent manner." J Cell Physiol **228**(7): 1473-1481.

Gogvadze, V., Orrenius, S. and Zhivotovsky, B. (2006). "Multiple pathways of cytochrome c release from mitochondria in apoptosis." Biochim Biophys Acta **1757**(5-6): 639-647.

Guo, Z. S., Liu, Z., Bartlett, D. L., Tang, D. and Lotze, M. T. (2013). "Life after death: targeting high mobility group box 1 in emergent cancer therapies." Am J Cancer Res **3**(1): 1-20.

Hager, E. D., Dziambor, H., Hohmann, D., Gallenbeck, D., Stephan, M. and Popa, C. (1999). "Deep hyperthermia with radiofrequencies in patients with liver metastases from colorectal cancer." Anticancer Res **19**(4C): 3403-3408.

Han, J., Zhong, C. Q. and Zhang, D. W. (2011). "Programmed necrosis: backup to and competitor with apoptosis in the immune system." Nat Immunol **12**(12): 1143-1149.

Harmon, B. V., Corder, A. M., Collins, R. J., Gobe, G. C., Allen, J., Allan, D. J. and Kerr, J. F. (1990). "Cell death induced in a murine mastocytoma by 42-47 degrees C heating in vitro: evidence that the form of death changes from apoptosis to necrosis above a critical heat load." Int J Radiat Biol **58**(5): 845-858.

Hegewisch-Becker, S., Gruber, Y., Corovic, A., Pichlmeier, U., Atanackovic, D., Nierhaus, A. and Hossfeld, D. K. (2002). "Whole-body hyperthermia (41.8 degrees C) combined with bimonthly oxaliplatin, high-dose leucovorin and 5-fluorouracil 48-hour continuous infusion in pretreated metastatic colorectal cancer: a phase II study." Ann Oncol **13**(8): 1197-1204.

Hellwig, C. T. and Rehm, M. (2012). "TRAIL signaling and synergy mechanisms used in TRAIL-based combination therapies." Mol Cancer Ther **11**(1): 3-13.

Hildebrandt, B., Wust, P., Ahlers, O., Dieing, A., Sreenivasa, G., Kerner, T., Felix, R. and Riess, H. (2002). "The cellular and molecular basis of hyperthermia." Crit Rev Oncol Hematol **43**(1): 33-56.

Horvath, I., Multhoff, G., Sonnleitner, A. and Vigh, L. (2008). "Membrane-associated stress proteins: more than simply chaperones." Biochim Biophys Acta **1778**(7-8): 1653-1664.

Horvath, I. and Vigh, L. (2010). "Cell biology: Stability in times of stress." Nature **463**(7280): 436-438.

Hou, C. H., Lin, F. L., Hou, S. M. and Liu, J. F. (2014). "Hyperthermia induces apoptosis through endoplasmic reticulum and reactive oxygen species in human osteosarcoma cells." Int J Mol Sci **15**(10): 17380-17395.

Issels, R. D., Lindner, L. H., Verweij, J., Wust, P., Reichardt, P., Schem, B. C., Abdel-Rahman, S., Daugaard, S., Salat, C., Wendtner, C. M., Vujaskovic, Z., Wessalowski, R., Jauch, K. W., Durr, H. R., Ploner, F., Baur-Melnyk, A., Mansmann, U., Hiddemann, W., Blay, J. Y. and Hohenberger, P. (2010). "Neo-adjuvant chemotherapy alone or with regional hyperthermia for localised high-risk soft-tissue sarcoma: a randomised phase 3 multicentre study." Lancet Oncol **11**(6): 561-570.

Jouan-Lanhouet, S., Arshad, M. I., Piquet-Pellorce, C., Martin-Chouly, C., Le Moigne-Muller, G., Van Herreweghe, F., Takahashi, N., Sergent, O., Lagadic-Gossmann, D., Vandenabeele, P., Samson, M. and Dimanche-Boitrel, M. T. (2012). "TRAIL induces necroptosis involving RIPK1/RIPK3-dependent PARP-1 activation." Cell Death Differ **19**(12): 2003-2014.

Kajihara, A., Takahashi, A., Ohnishi, K., Imai, Y., Yamakawa, N., Yasumoto, J., Ohnishi, T. and Kirita, T. (2008). "Protein microarray analysis of apoptosis-related protein expression following heat shock in human tongue squamous cell carcinomas containing different p53 phenotypes." Int J Hyperthermia **24**(8): 605-612.

Kepp, O., Galluzzi, L., Martins, I., Schlemmer, F., Adjemian, S., Michaud, M., Sukkurwala, A. Q., Menger, L., Zitvogel, L. and Kroemer, G. (2011). "Molecular determinants of immunogenic cell death elicited by anticancer chemotherapy." Cancer Metastasis Rev **30**(1): 61-69.

Kepp, O., Tesniere, A., Schlemmer, F., Michaud, M., Senovilla, L., Zitvogel, L. and Kroemer, G. (2009). "Immunogenic cell death modalities and their impact on cancer treatment." Apoptosis **14**(4): 364-375.

Kerr, J. F., Wyllie, A. H. and Currie, A. R. (1972). "Apoptosis: a basic biological phenomenon with wide-ranging implications in tissue kinetics." Br J Cancer **26**(4): 239-257.

Kroemer, G., El-Deiry, W. S., Golstein, P., Peter, M. E., Vaux, D., Vandenabeele, P., Zhivotovsky, B., Blagosklonny, M. V., Malorni, W., Knight, R. A., Piacentini, M., Nagata, S. and Melino, G. (2005). "Classification of cell death: recommendations of the Nomenclature Committee on Cell Death." Cell Death Differ **12 Suppl 2**: 1463-1467.

Kroemer, G., Galluzzi, L., Kepp, O. and Zitvogel, L. (2013). "Immunogenic cell death in cancer therapy." Annu Rev Immunol **31**: 51-72.

Kroemer, G., Galluzzi, L., Vandenabeele, P., Abrams, J., Alnemri, E. S., Baehrecke, E. H., Blagosklonny, M. V., El-Deiry, W. S., Golstein, P., Green, D. R., Hengartner, M., Knight, R. A., Kumar, S., Lipton, S. A., Malorni, W., Nunez, G., Peter, M. E., Tschopp, J., Yuan, J., Piacentini, M., Zhivotovsky, B. and Melino, G. (2009). "Classification of cell death: recommendations of the Nomenclature Committee on Cell Death 2009." Cell Death Differ **16**(1): 3-11.

Krysko, D. V., Garg, A. D., Kaczmarek, A., Krysko, O., Agostinis, P. and Vandenabeele, P. (2012). "Immunogenic cell death and DAMPs in cancer therapy." Nat Rev Cancer **12**(12): 860-875.

Krysko, O., Love Aaes, T., Bachert, C., Vandenabeele, P. and Krysko, D. V. (2013). "Many faces of DAMPs in cancer therapy." Cell Death Dis **4**: e631.

Ladoire, S., Hannani, D., Vetizou, M., Locher, C., Aymeric, L., Apetoh, L., Kepp, O., Kroemer, G., Ghiringhelli, F. and Zitvogel, L. (2013). "Cell-Death-Associated Molecular Patterns As Determinants of Cancer Immunogenicity." Antioxid Redox Signal.

Liang, H., Zhan, H. J., Wang, B. G., Pan, Y. and Hao, X. S. (2007). "Change in expression of apoptosis genes after hyperthermia, chemotherapy and radiotherapy in human colon cancer transplanted into nude mice." World J Gastroenterol **13**(32): 4365-4371.

Lui, P. C., Fan, Y. S., Xu, G., Ngai, C. Y., Fung, K. P., Tse, G. M., Yu, A. M. and Li, J. Y. (2010). "Apoptotic and necrotic effects of tumour necrosis factor-alpha potentiated with hyperthermia on L929 and tumour necrosis factor-alpha-resistant L929." Int J Hyperthermia **26**(6): 556-564.

Makizumi, R., Yang, W. L., Owen, R. P., Sharma, R. R. and Ravikumar, T. S. (2008). "Alteration of Drug Sensitivity in Human Colon Cancer Cells after Exposure to Heat: Implications for Liver Metastasis Therapy using RFA and Chemotherapy." Int J Clin Exp Med **1**(2): 117-129.

Martins, I., Michaud, M., Sukkurwala, A. Q., Adjemian, S., Ma, Y., Shen, S., Kepp, O., Menger, L., Vacchelli, E., Galluzzi, L., Zitvogel, L. and Kroemer, G. (2012). "Premortem autophagy determines the immunogenicity of chemotherapy-induced cancer cell death." Autophagy **8**(3): 413-415.

Mátay, G. and Zombory, L. (2000). A rádiófrekvenciás sugárzás élettani hatásai és orvosbiológiai alkalmazásai, Műegyetemi Kiadó.

Menger, L., Vacchelli, E., Adjemian, S., Martins, I., Ma, Y., Shen, S., Yamazaki, T., Sukkurwala, A. Q., Michaud, M., Mignot, G., Schlemmer, F., Sulpice, E., Locher, C., Gidrol, X., Ghiringhelli, F., Modjtahedi, N., Galluzzi, L., Andre, F., Zitvogel, L., Kepp, O. and Kroemer, G. (2012). "Cardiac glycosides exert anticancer effects by inducing immunogenic cell death." Sci Transl Med **4**(143): 143ra199.

Moreno-Ramirez, D., de la Cruz-Merino, L., Ferrandiz, L., Villegas-Portero, R. and Nieto-Garcia, A. (2010). "Isolated limb perfusion for malignant melanoma: systematic review on effectiveness and safety." Oncologist **15**(4): 416-427.

Mroz, P., Hashmi, J. T., Huang, Y. Y., Lange, N. and Hamblin, M. R. (2011). "Stimulation of anti-tumor immunity by photodynamic therapy." Expert Rev Clin Immunol **7**(1): 75-91.

Multhoff, G. (2007). "Heat shock protein 70 (Hsp70): membrane location, export and immunological relevance." Methods **43**(3): 229-237.

Multhoff, G. and Hightower, L. E. (2011). "Distinguishing integral and receptor-bound heat shock protein 70 (Hsp70) on the cell surface by Hsp70-specific antibodies." Cell Stress Chaperones **16**(3): 251-255.

Natarajan, S. K. and Becker, D. F. (2012). "Role of apoptosis-inducing factor, proline dehydrogenase, and NADPH oxidase in apoptosis and oxidative stress." Cell Health Cytoskelet **2012**(4): 11-27.

Nicotera, P. (2002). "Apoptosis and age-related disorders: role of caspase-dependent and caspase-independent pathways." Toxicol Lett **127**(1-3): 189-195.

Nishida, T., Akagi, K. and Tanaka, Y. (1997). "Correlation between cell killing effect and cell membrane potential after heat treatment: analysis using fluorescent dye and flow cytometry." Int J Hyperthermia **13**(2): 227-234.

Norberg, E., Orrenius, S. and Zhivotovsky, B. (2010). "Mitochondrial regulation of cell death: processing of apoptosis-inducing factor (AIF)." Biochem Biophys Res Commun **396**(1): 95-100.

O'Rourke, A. P., Lazebnik, M., Bertram, J. M., Converse, M. C., Hagness, S. C., Webster, J. G. and Mahvi, D. M. (2007). "Dielectric properties of human normal, malignant and cirrhotic liver tissue: in vivo and ex vivo measurements from 0.5 to 20 GHz using a precision open-ended coaxial probe." Phys Med Biol **52**(15): 4707-4719.

Overgaard, J. (1984). "Formula to estimate the thermal enhancement ratio of a single simultaneous hyperthermia and radiation treatment." Acta Radiol Oncol **23**(2-3): 135-139.

Perez, C. A., Pajak, T., Emami, B., Hornback, N. B., Tupchong, L. and Rubin, P. (1991). "Randomized phase III study comparing irradiation and hyperthermia with irradiation alone in superficial measurable tumors. Final report by the Radiation Therapy Oncology Group." Am J Clin Oncol **14**(2): 133-141.

Pethig, R., Gascoyne, P. R., McLaughlin, J. A. and Szent-Gyorgyi, A. (1984). "Interaction of the 2,6-dimethoxysemiquinone and ascorbyl free radicals with Ehrlich ascites cells: a probe of cell-surface charge." Proc Natl Acad Sci U S A **81**(7): 2088-2091.

Pfister, K., Radons, J., Busch, R., Tidball, J. G., Pfeifer, M., Freitag, L., Feldmann, H. J., Milani, V., Issels, R. and Multhoff, G. (2007). "Patient survival by Hsp70 membrane phenotype: association with different routes of metastasis." Cancer **110**(4): 926-935.

Raoof, M., Cisneros, B. T., Corr, S. J., Palalon, F., Curley, S. A. and Koshkina, N. V. (2013). "Tumor selective hyperthermia induced by short-wave capacitively-coupled RF electric-fields." PLoS One **8**(7): e68506.

Richel, O., Zum Vorde Sive Vording, P. J., Rietbroek, R., Van der Velden, J., Van Dijk, J. D., Schilthuis, M. S. and Westermann, A. M. (2004). "Phase II study of carboplatin and whole body hyperthermia (WBH) in recurrent and metastatic cervical cancer." Gynecol Oncol **95**(3): 680-685.

Robert, J. (2003). "Evolution of heat shock protein and immunity." Dev Comp Immunol **27**(6-7): 449-464.

Rong, Y. and Mack, P. (2000). "Apoptosis induced by hyperthermia in Dunn osteosarcoma cell line in vitro." Int J Hyperthermia **16**(1): 19-27.

Sachamitr, P. and Fairchild, P. J. (2012). "Cross presentation of antigen by dendritic cells: mechanisms and implications for immunotherapy." Expert Rev Clin Immunol **8**(6): 547-555.

Scheffer, S. R., Nave, H., Korangy, F., Schlote, K., Pabst, R., Jaffee, E. M., Manns, M. P. and Greten, T. F. (2003). "Apoptotic, but not necrotic, tumor cell vaccines induce a potent immune response in vivo." Int J Cancer **103**(2): 205-211.

Scholoz, B. and Anderson, R. (2000). "On electrical impedance scanning-principles and simulations." Electromedica **68**: 35-44.

Schwan, H. P. (1957). "Electrical properties of tissue and cell suspensions." Adv Biol Med Phys **5**: 147-209.

Shchepotin, I. B., Soldatenkov, V., Wroblewski, J. T., Surin, A., Shabahang, M., Buras, R. R., Nauta, R. J., Pulyaeva, H. and Evans, S. R. (1997). "Apoptosis induced by hyperthermia and verapamil in vitro in a human colon cancer cell line." Int J Hyperthermia **13**(5): 547-557.

Spisek, R., Charalambous, A., Mazumder, A., Vesole, D. H., Jagannath, S. and Dhodapkar, M. V. (2007). "Bortezomib enhances dendritic cell (DC)-mediated induction of immunity to human myeloma via exposure of cell surface heat shock protein 90 on dying tumor cells: therapeutic implications." Blood **109**(11): 4839-4845.

Stolfi, C., Pallone, F. and Monteleone, G. (2012). "Molecular Targets of TRAIL-Sensitizing Agents in Colorectal Cancer." Int J Mol Sci **13**(7): 7886-7901.

Sun, X., Li, X. F., Russell, J., Xing, L., Urano, M., Li, G. C., Humm, J. L. and Ling, C. C. (2008). "Changes in tumor hypoxia induced by mild temperature hyperthermia as assessed by dual-tracer immunohistochemistry." Radiother Oncol **88**(2): 269-276.

Szasz, A., Szasz, N. and Szasz, O. (2010). Oncothermia: Principles and Practices: Principles and Practices, Springer.

Szasz, A., Szasz, O. and Szasz, N. (2002). "Onkotermia Fizika a rák ellen." Fizikai szemle **52**(2): 45-52.

Tait, S. W. and Green, D. R. (2010). "Mitochondria and cell death: outer membrane permeabilization and beyond." Nat Rev Mol Cell Biol **11**(9): 621-632.

Tamamoto, T., Yoshimura, H., Takahashi, A., Asakawa, I., Ota, I., Nakagawa, H., Ohnishi, K., Ohishi, H. and Ohnishi, T. (2003). "Heat-induced growth inhibition and apoptosis in transplanted human head and neck squamous cell carcinomas with different status of p53." Int J Hyperthermia **19**(6): 590-597.

Tesniere, A., Schlemmer, F., Boige, V., Kepp, O., Martins, I., Ghiringhelli, F., Aymeric, L., Michaud, M., Apetoh, L., Barault, L., Mendiboure, J., Pignon, J. P., Jooste, V., van Endert, P., Ducreux, M., Zitvogel, L., Piard, F. and Kroemer, G. (2010). "Immunogenic death of colon cancer cells treated with oxaliplatin." Oncogene **29**(4): 482-491.

Trabulsi, N. H., Patakfalvi, L., Nassif, M. O., Turcotte, R. E., Nichols, A. and Meguerditchian, A. N. (2012). "Hyperthermic isolated limb perfusion for extremity soft tissue sarcomas: systematic review of clinical efficacy and quality assessment of reported trials." J Surg Oncol **106**(8): 921-928.

Ullrich, E., Bonmort, M., Mignot, G., Kroemer, G. and Zitvogel, L. (2008). "Tumor stress, cell death and the ensuing immune response." Cell Death Differ **15**(1): 21-28.

Vandenabeele, P., Galluzzi, L., Vanden Berghe, T. and Kroemer, G. (2010). "Molecular mechanisms of necroptosis: an ordered cellular explosion." Nat Rev Mol Cell Biol **11**(10): 700-714.

Vanlangenakker, N., Vanden Berghe, T. and Vandenabeele, P. (2012). "Many stimuli pull the necrotic trigger, an overview." Cell Death Differ **19**(1): 75-86.

Wang, S. (2010). "TRAIL: a sword for killing tumors." Curr Med Chem **17**(29): 3309-3317.

Westermann, A. M., Wiedemann, G. J., Jager, E., Jager, D., Katschinski, D. M., Knuth, A., Vorde Sive Vording, P. Z., Van Dijk, J. D., Finet, J., Neumann, A., Longo, W., Bakhshandeh, A., Tiggelaar, C. L., Gillis, W., Bailey, H., Peters, S. O. and Robins, H. I. (2003). "A Systemic Hyperthermia Oncologic Working Group trial. Ifosfamide, carboplatin, and etoposide combined with 41.8 degrees C whole-body hyperthermia for metastatic soft tissue sarcoma." Oncology **64**(4): 312-321.

Wismeth, C., Dudel, C., Pascher, C., Ramm, P., Pietsch, T., Hirschmann, B., Reinert, C., Proescholdt, M., Rummele, P., Schuierer, G., Bogdahn, U. and Hau, P. (2010). "Transcranial electro-hyperthermia combined with alkylating chemotherapy in patients with relapsed high-grade gliomas: phase I clinical results." J Neurooncol **98**(3): 395-405.

Wust, P., Hildebrandt, B., Sreenivasa, G., Rau, B., Gellermann, J., Riess, H., Felix, R. and Schlag, P. M. (2002). "Hyperthermia in combined treatment of cancer." Lancet Oncol **3**(8): 487-497.

Yonezawa, M., Otsuka, T., Matsui, N., Tsuji, H., Kato, K. H., Moriyama, A. and Kato, T. (1996). "Hyperthermia induces apoptosis in malignant fibrous histiocytoma cells in vitro." Int J Cancer **66**(3): 347-351.

Zhou, J., Wang, X., Du, L., Zhao, L., Lei, F., Ouyang, W., Zhang, Y., Liao, Y. and Tang, J. (2011). "Effect of hyperthermia on the apoptosis and proliferation of CaSki cells." Mol Med Rep **4**(1): 187-191.

Zou, Y. and Guo, Z. (2003). "A review of electrical impedance techniques for breast cancer detection." Med Eng Phys **25**(2): 79-90.

DOI:10.14753/SE.2015.1802

12. BIBLIOGRAPHY OF THE CANDIDATE'S PUBLICATIONS

Publication related to the PhD thesis

Andocs, G., Meggyeshazi, N., Balogh, L., Spisak, S., Maros, M. E., Balla, P., Kiszner, G., Teleki, I., Kovago, C. and Krenacs, T. (2014). "Upregulation of heat shock proteins and the promotion of damage-associated molecular pattern signals in a colorectal cancer model by modulated electrohyperthermia." Cell Stress Chaperones. (Ahead of print)
Andocs G. and Meggyeshazi N. are equally contributed to this work.

Meggyeshazi, N., Andocs, G., Balogh, L., Balla, P., Kiszner, G., Teleki, I., Jeney, A. and Krenacs, T. (2014). "DNA fragmentation and caspase-independent programmed cell death by modulated electrohyperthermia." Strahlenther Onkol. (Ahead of print)

Publication not related to the PhD thesis

Teleki, I., Szasz, A. M., Maros, M. E., Gyorffy, B., Kulka, J., Meggyeshazi, N., Kiszner, G., Balla, P., Samu, A. and Krenacs, T. (2014). "Correlations of differentially expressed gap junction connexins cx26, cx30, cx32, cx43 and cx46 with breast cancer progression and prognosis." PLoS One 9(11): e112541.

Penzvalto, Z., Lanczky, A., Lenart, J., Meggyeshazi, N., Krenacs, T., Szoboszlai, N., Denkert, C., Pete, I. and Gyorffy, B. (2014). "MEK1 is associated with carboplatin resistance and is a prognostic biomarker in epithelial ovarian cancer." BMC Cancer 14: 837.

Kiszner, G., Wichmann, B., Nemeth, I. B., Varga, E., Meggyeshazi, N., Teleki, I., Balla, P., Maros, M. E., Penksza, K. and Krenacs, T. (2014). "Cell cycle analysis can differentiate thin melanomas from dysplastic nevi and reveals accelerated replication in thick melanomas." Virchows Arch 464(5): 603-612.

Stelkovics, E., Kiszner, G., Meggyeshazi, N., Korom, I., Varga, E., Nemeth, I., Molnar, J., Marczinovits, I. and Krenacs, T. (2013). "Selective in situ protein expression profiles correlate with distinct phenotypes of basal cell carcinoma and squamous cell carcinoma of the skin." Histol Histopathol 28(7): 941-954.

Citable abstracts

Meggyeshazi, N; Andocs, G; Balogh, L; Krenacs, T (2011) “DNA fragmentation-driven tumor cell degradation induced by modulated electro-hyperthermia” Virchows Arch 459 (Suppl 1):S204-205

Meggyeshazi, N; Andocs, G; Krenacs, T (2012) “Modulated electro-hyperthermia induced programmed cell death in HT29 colorectal carcinoma xenograft” Virchows Arch 461 (Suppl 1):S131–S132

Teleki, I, .Szasz, M. A., Kulka, J. Meggyeshazi, N.;Kiszner, G.; Balla, B.; Krenacs, T. (2013) “Expression and potential involvement of connexins in breast cancer progression” Virchows Arch 463 (2) 260-261

Kiszner, G., Teleki, I.; Meggyeshazi, N.; Balla, P.; Maros, M. E.; Nemeth, I. B.; Varga, E.; Korom, I.; Krenacs, T. (2013) “Exploring connexin expression in melanocytic tumors” Virchows Arch 463 (2) 284

Meggyeshazi, N.; Andocs, G.; Spisak, S.; Kiszner, G.; Balla, P.; Balogh, L.; Krenacs, T. (2013) “Modulated electrohyperthermia causes caspase independent programmed cell death in HT29 colon cancer xenografts” Virchows Arch 463 (2) 329

DOI:10.14753/SE.2015.1802

13. ACKNOWLEDGEMENTS

I am thankful for Professor Dr András Matolcsy for hosting me in his Institution.
I am utterly grateful for Dr. Tibor Krenács for the possibility to work in his laboratory and for his helpful advices and support.
I am thankful for all the members of the laboratory first of all Edit Parsch whose technical help was crucial for my work, for Dr. Ivett Teleki, Dr. Maté Maros, Dr. Gergő Kiszner and Péter Balla for their remarks and friendly conversations.
I am utterly grateful for Professor Dr. András Jeney for his advices, support and friendly conversations.
I am grateful for all the members of the Department who at any how helped me throughout my work.
I am thankful for Dr. Lajos Balogh for his help in the animal experiments.
I am also grateful to Professor Dr. Andras Szasz for support and useful advice throughout my project.
At last but not least I am thankful from the bottom of my heart for all the members of my family for their lifetime love and support.